Structure of Conjugated Bile Salt−Fatty Acid−Monoglyceride Mixed Colloids: Studies by Small-Angle Neutron Scattering

Rex P. Hjelm*

Manuel Lujan Jr. Neutron Scattering Center, Los Alamos Neutron Science Center, Los Alamos National Laboratory, Los Alamos, New Mexico 87545-1663

Claudio D. Schteingart and Alan F. Hofmann

Department of Medicine, School of Medicine, University of California, San Diego, La Jolla, California 92093-0813

P. Thiyagarajan

Intense Pulsed Neutron Source, Argonne National Laboratory, 9700 S. Cass Avenue, Argonne, Illinois 60439

Received: June 25, 1999; In Final Form: October 29, 1999

The structures of particles found in isotropic phases of mixed surfactant systems consisting of conjugated bile salts and fatty lipids were assessed using small-angle neutron scattering. The conjugated bile salts were either cholylglycine or chenodeoxycholylglycine. The fatty lipids were mixtures of oleate and oleic acid either alone or with monoolein. The scattering data suggested that both particle interactions and polydispersity must be modeled in these systems. Particle interactions were modeled using the reduced mean spherical approximation and the decoupling approximation. Maximum entropy was used to characterize the polydispersity. A self-consistent analysis of the scattering was arrived at by making an initial estimate of particle size and shape using derivative−log and Guinier analysis and refining the estimates by analyzing the particle interactions and polydispersity and iterating. The scattering at high total lipid concentrations was consistent with globular mixed micelles with repulsive electrostatic interactions. The globular mixed micelles in these systems were similar in size and shape to those observed previously in conjugated bile salt mixtures with either egg yolk phosphatidylcholine or monoolein. Solutions of cholylglycine with monoolein and oleate/oleic acid underwent a transition to vesicles at lower concentrations. This behavior was similar to those observed in conjugated bile salts with either egg yolk phosphatidylcholine or monoolein. Cholylglycine mixtures with oleate/oleic showed somewhat different behavior at lower concentrations, since there was also evidence for coexistence of elongated and tabletlike micelles. Despite these differences, there were sufficient similarities in the particle morphologies of these and other conjugated bile salt−fatty lipid systems to suggest a common mode of self-assembly. These solutions are models for bile in the bilary system and intestine content during triglyceride digestion; the common themes of self-assembly have implications for the physiology of lipid solubilization in bile as well as intestinal absorption of dietary lipids.

Introduction

Investigations of mixed surfactant systems have shown a rich variety of phases. The phases include isotropic phases consisting of quasi-spherical, cylindrical, disklike, and rod or ribbonlike mixed micelles and mixed vesicles.[1−4] The rods or ribbons may become extremely long, forming wormlike micelles.[3,5−7] There are also liquid crystalline phases with lamellar and hexagonal geometries and different bicontinuous morphologies.[2,8−10] The latter includes sponge and cubic phases. The overall theme of self-assembly in these systems is understood in terms of the hydrophobic effect, hydrophilic head interactions, and molecular packing parameters.[11−13] However, despite the large literature on this subject, the determinants of important details of the behavior of these systems are only just emerging. Detailed analysis of the phases is needed to assess the way in which the interplay of molecular shapes and interactions affects the balance of the hydrophobic effect and molecular interactions.

We have been studying the isotropic phases of mixed colloids consisting of one of the bile salts, cholylglycine, chenodeoxycholylglycine or cholyltaurine, together with one of the fatty lipids, egg yolk phosphatidylcholine (EYPC), dipalmatoylphosphatidylcholine (DPPC), or monoolein.[1,14−19] These bile salt−fatty lipid systems, which we describe as asymmetric, have amphiphiles with very different solubility and morphology. These are distinguished from the symmetric systems, which have been extensively studied recently,[2−4,9] consisting of surfactants having similar geometry and solubility. In our asymmetric systems, among the relatively insoluble fatty lipids, monoolein has a neutral headgroup and one flexible fatty acid tail. DPPC and EYPC have zwitterionic headgroups at near-neutral pH and two flexible fatty acid tails. The significantly more soluble

* To whom correspondence should be sent. Phone: 1-505-665-2372. Fax: 1-505-665-2676. E-mail: Hjelm@lanl.gov.

10.1021/jp992157n CCC: $19.00
Published on Web 12/22/1999

conjugated bile salts have a completely charged headgroup at neutral pH. The bile salt bodies consist of a rigid steroid nucleus that has hydrophilic character on one side, due to the presence of either two (chenodeoxycholylglycine) or three (the cholyl conjugates) hydroxyl groups, and hydrophobic character on the other. Not surprisingly, the phase maps of the asymmetric systems are substantially different from those of the symmetric systems.

The bile salt−fatty lipid systems are also interesting because these mixtures are models for the structure and action of bile—the fluid vehicle for lipid transport from the liver to the intestine as well as intestinal content during lipid absorption. Models of the digestive process in the small intestine must simulate its actual content if studies of the physical chemistry are to have biological relevance. Ultimately, such studies should clarify the process of emulsification of insoluble dietary triglyceride, its hydrolysis by pancreatic lipase, and micellar solubilization of monoglyceride and fatty acids. This is a challenge, since the intestine contains a highly complex mixture of dietary materials, their digestion products, enzymes, and bile components.[20−22] On the other hand, the models must be simple to be amenable to effective physical chemical examination. We have selected model systems of conjugated bile salts and fatty lipids that are within the range of values found in intestinal content on digestion of dietary triglycerides.[20,23] Thus, these findings are likely to be relevant to the understanding of fat digestion and absorption. With a unifying theme of particle formation, inclusion of other factors can be approached as perturbations on this theme.

We used small-angle neutron scattering (SANS) to determine particle size and shape and molecular arrangement as a function of total lipid concentration[1,14−19] These and similar studies[6,24,25] showed that SANS is a powerful tool for structural investigation of these colloids, providing an essential complement to light scattering,[5,7,8,26,27] hydrodynamic,[28] NMR,[8,29,30] and cryotransmission electron microscopy[10,31,32] measurements.

To understand the nature of self-assembly in mixed systems, it is necessary to characterize all aspects of the system, including particle morphology, polydispersity, and interactions. This is a difficult problem. Here, we introduce methods to directly address some of the complexities of the mixed systems and use these methods to dissect and analyze the structures and interactions present in complex, polydisperse mixtures.

In the present study, we extended our SANS measurements to include the isotropic phases of the conjugated bile salts, chenodeoxycholylglycine or cholylglycine, with either monoolein and oleic acid (and oleate, its conjugate anion) or oleic acid and oleate alone. Incorporation of oleate adds charge to the micelle, and both oleate and oleic acid have a single fatty tail but have a substantially smaller headgroup than monoolein. Oleate, because of the radically different headgroup, a carboxylate moiety, should provide further evidence on the molecular factors that govern self-assembly in these systems. Monoolein and oleate are the predominant triglyceride digestion products; thus, the inclusion of oleate complements our previous work on the previous bile model systems of conjugated bile salts with either EYPC or monoolein.

We find that the concentration-dependent particle structures seen in solutions of cholylglycine with monoolein and oleate/oleic acid are very similar to those that occur in analogous solutions with EYPC or monoolein. Chenodeoxycholylglycine with monoolein and oleate/oleic acid or just oleate/oleic acid also behaves similarly to the EYPC and monoolein counterparts. However, cholylglycine with oleate/oleic acid shows considerable differences from the other systems in particle morphology. These results support the notion that the positive curvature, needed to stabilize the prolate cylinder morphology of the mixed micelles, provided by the bile salts is the predominate factor determining the shape of the micelles. This effect is sufficiently strong to counter the negative curvature of monoolein and oleate. However, the effect is much more tenuous when the more soluble cholylglycine is present and mass action, which determines the amount of bile salt in the micelle, dominates the particle form. Our results support the hypothesis, forwarded in our previous work, that the conservation of bile particle structure is of major physiological importance.

Materials and Methods

Materials. Stock solutions of bile salt with monoolein, oleic acid, and Na oleate were prepared by the addition of the sodium salts of the bile acids, cholylglycine (3α,7α,12α-trihydroxy-5β-cholan-24-oyl glycine, molecular weight, $W = 488$ D), or chenodeoxycholylglycine (3α,7α-dihydroxy-5β-cholan-24-oyl glycine, $W = 472$ D) with 6.4 mM each of monoolein (glyceryl-1-monoctadecanoate, $W = 357$ D), oleic acid (*cis*-9-octadecanoid acid, $W = 282$ D), and sodium oleate in a D_2O buffer containing 20 mM PIPES (the pH was measured as 6.5 in a similar solution containing H_2O) and enough NaCl to give a total sodium concentration of 150 mM. The final concentration of bile salt in the respective stocks was 20 mM cholylglycine and 16.4 mM chenodeoxycholylglycine. A second stock of each was produced by addition of 4 mL of D_2O buffer to 8 mL of the first stock. All other samples were made from the second stock by addition of D_2O buffer. The total lipid concentrations in the cholylglycine samples were 15.7, 10.5, 7.0, 5.2, 4.2, 2.6, 2.1, 0.52, and 0.39 g/L, with a molar ratio of fatty lipid to bile salt, $\Gamma = 0.96$. The samples containing chenodeoxycholylglycine had 13.6, 9.1, 6.0, 4.5, 3.6, 2.3, 1.8, and 0.45 g/L total lipid, with $\Gamma = 1.17$.

Mixtures of bile salts with cholylglycine, sodium oleate, and oleic acid were prepared by dilution from a stock solution in D_2O buffer (above) containing 21.8 mM cholylglycine and 10.3 mM each of Na oleate and oleic acid ($\Gamma = 0.94$). Those with chenodeoxycholylglycine contained 20.9 mM chenodeoxycholylglycine and 11.7 mM each of Na oleate and oleic acid ($\Gamma = 1.12$). Each 16.7 g/L stock was diluted to 10.0 g/L total lipid to produce a second stock that was then further diluted to 6.6, 5.0, 4.0, 2.5, 2.0, 1.0, and 0.375 g/L with additional D_2O buffer. Sometimes acid soap precipitated from these solutions.[33] When this happened, the samples were returned to their original clear state by heating and then mixing the sample with a vortex.

Small-Angle Neutron Scattering. Small-angle neutron scattering measurements were done on the 30 M SANS camera, NG7SANS, at the National Institutes of Standards and Technology (NIST), Gaithersburg, Maryland and on the time-of-flight (TOF) SANS, the small-angle diffractometer, SAD, at the intense pulsed neutron source (IPNS) at Argonne National Laboratory. Data from the TOF instrument were reduced using methods described elsewhere.[34,35] Intensity measurements, $I(Q)$, were placed on an absolute scale of differential cross section per milligram total lipid, $cm^2\ mg^{-1}$, using secondary standards: mixtures of polystyrene and deuterated polystyrene or silica gels. Here, Q is the momentum transferred to the scattered neutron. Its magnitude is $Q = (4\pi/\lambda)\sin\theta$, where λ is the wavelength of the neutron and 2θ is the scattering angle.

Data Analysis. Under ideal conditions of particles uncorrelated in position and orientation the SANS $I(Q)$ data are proportional to a spherical-averaged form factor, $\langle P(Q)\rangle =$

$\langle|F(Q)|^2\rangle$, where $F(Q)$ is the Fourier transform of the particle structure, $\rho(\mathbf{r})$. In the present study, we modeled the data using $\langle P(Q)\rangle$ for two distinct particle morphologies: straight circular cylinders and vesicles. For a cylinder with radius R and height H, $\langle P(Q)\rangle$ is given by

$$\langle P(Q|R,H)\rangle = 16\int_0^{2\pi} \frac{\sin^2(QH/2\cos\theta)}{Q^2H^2\cos^2\theta}\frac{J_1^2(QR\sin\theta)}{Q^2R^2\sin^2\theta}\sin\theta\,\mathrm{d}\theta \quad (1)$$

In eq 1, J_1 is a first-order Bessel function of the first kind. For a spherical vesicle of radius R and thickness $t = R - r$, the form factor is given by

$$\langle P(Q|R,r)\rangle = 9\frac{\{R^2j_1(QR) - r^2j_1(Qr)\}^2}{Q^2(R^3 - r^3)^2} \quad (2)$$

Here, j_1, is the spherical Bessel function of the first kind.

In real systems, there is often polydispersity; thus, the form factor used to model the scattering must be an appropriate average over the population, $\overline{\langle P(Q)\rangle}$. Particle interactions can also be present that alters the observed scattering. Taking into account both of these complicating factors, spheroid particle scattering intensity is approximated by

$$I(Q) \propto S'(Q)\overline{\langle P(Q)\rangle} \quad (3)$$

where $S'(Q)$ is the effective structure factor representing the contributions to the scattering due to correlations between particles (see eqs 11−15).[36] Equation 3, the decoupling approximation, is also used as an approximation for nonspherical particles (see eqs 16 and 17).[36]

Quantitative analysis of particle size and shape starts with the Guinier approximations. We have introduced the generalized Guinier approximations for particle form factors[17]

$$\langle P(Q)\rangle = \left.\begin{cases}1; & \alpha = 0\\ \alpha\pi\,\mathrm{Q}^{-\alpha}; & \alpha = 1,2\end{cases}\right\}\Delta M_{\alpha 0}\exp\left(-\frac{R_\alpha{}^2\mathrm{Q}^2}{3-\alpha}\right) \quad (4)$$

Moreover, the derivative of $\ln[I(Q)]$ with respect to $\ln Q$ is[17]

$$\frac{\mathrm{d}\ln\langle P(Q)\rangle}{\mathrm{d}\ln(Q)} = \frac{Q}{\langle P(Q)\rangle}\frac{\mathrm{d}\langle P(Q)\rangle}{\mathrm{d}Q} = -\alpha - \frac{2}{3-\alpha}\mathrm{R}_\alpha{}^2\mathrm{Q}^2 \quad (5)$$

Equations 4 and 5 state that there are Q domains, corresponding to length scales as Q^{-1}, from which the particle dimension or shape, α, the radius of gyration, R_α, and the prefactor, $\Delta M_{\alpha 0}$, characteristic of α can be inferred. α (eqs 4 and 5) has a value of 0 for a Q domain such that $QR_g < 1-1.3$ (the larger applies when the particle is known to be a spheroid), where R_g is the particle radius of gyration (computed about the particle centroid). In this case, the prefactor is ΔM_0, the excess differential cross section per unit mass ($\mathrm{cm}^2\ \mathrm{g}^{-1}$) of a particle. For most SANS instruments such a Q domain can only be accessed for globular particles. If the particle has one dimension of length L, that is, much larger than the others (i.e., elongated, rodlike, or wormlike), then there is a Q domain such that $QR_c < 1 \ll QL$, where $\alpha = 1$. Here, R_c is the radius of gyration (computed about a line centered along L) of the cross section perpendicular to L. If these conditions apply, the prefactor is Δm_0 , the excess differential cross section per unit length per unit mass ($\mathrm{cm}^2\ \text{Å}^{-1}\ \mathrm{g}^{-1}$). Finally, for planar shapes, including single bilayer vesicles (SLV's), with two locally large dimensions, D, and planar cross-sectional radius of gyration (computed about a central plain), R_d, there may be a region of Q such that $QR_d < 1 \ll QD$, where $\alpha = 2$. For such planar structures, the prefactor is the excess differential cross section per unit area per unit mass ($\mathrm{cm}^2\ \text{Å}^2\ \mathrm{g}^{-1}$) of a sheet, $\Delta\mu_0$. Such domains can be found and the corresponding α and $R_\alpha{}^2$ computed using a plot of $[Q/I(Q)]$-$[\mathrm{d}I(Q)/\mathrm{d}Q]$ versus Q^2 (eq 5). A region of Q that gives a straight line extrapolating to an appropriate integral value of α identifies such a domain. The value of α is diagnostic of the particle shape. The slope of the line will be ${}^2/_{(3-\alpha)}R_\alpha{}^2$, giving the characteristic radius of gyration. We have termed this form of the Guinier approximation, the derivative−log(D−L) analysis. Having used this procedure to identify candidate Q domains for Guinier analysis, we can then use the appropriate form of eq 4 to determine ΔM_α and to make another estimate of R_α.

This procedure is useful in complex cases, such as when the particle population contains objects of more than one type. Another example is when more than one type of Guinier analysis is used to characterize a particle, provided the Q domains with different α are well separated. This procedure is also useful when particle interactions contribute to the scatter. Equations 4 and 5 will give the same estimate of R_α if and only if $S'(Q) \cong 1$, as from eqs 3 and 5,

$$\frac{Q}{I(Q)}\frac{\mathrm{d}I(Q)}{\mathrm{d}Q} = \frac{Q}{S'(Q)}\frac{\mathrm{d}S'(Q)}{\mathrm{d}Q} + \frac{Q}{\langle P(Q)\rangle}\frac{\mathrm{d}\langle P(Q)\rangle}{\mathrm{d}Q} \quad (6)$$

Otherwise, the Guinier and D−L treatments will give systematic errors of opposite sign for R_α.

For polydispersed systems we take into account that the observed intensity is the sum of scattering from all the particles present in solution,

$$\overline{\langle P(Q)\rangle} = \frac{\int\int f(p_1,p_2)\,\Delta\rho^2(p_1,p_2)\,V^2(p_1,p_2)\,\langle P(Q|p_1p_2)\rangle\,\mathrm{d}p_1\,\mathrm{d}p_2}{\overline{(\Delta\rho V^2)}} \quad (7)$$

where p_1 and p_2 are structural parameters (the radius and thickness of a vesicle, say) and f is the joint probability density function (PDF). In eq 7, $\overline{(\Delta\rho V)^2} = \int\int f(p_1,p_2)\,\Delta\rho^2(p_1,p_2)\,V^2(p_1,p_2)\,\mathrm{d}p_1\,\mathrm{d}p_2$. The particle volume is V and the contrast is $\Delta\rho = \bar{\rho} - \rho_s$, the difference between the average scattering length density of the particle, $\bar{\rho}$, and the solvent, ρ_s. From eq 7, the parameters of eqs 4 and 5 are averages given by

$$\overline{\Delta M_0} = \frac{\int\int f(p_1,p_2)\,\Delta\rho^2(p_1,p_2)\,V^2(p_1,p_2)\,\mathrm{d}p_1\,\mathrm{d}p_2}{\overline{M} + N_0{}^{-1}\overline{N_L}W_B(\Gamma^{-1} - \gamma^{-1})} \quad (8)$$

and

$$\overline{R_{g_z}{}^2} = \frac{\int\int f(p_1,p_2)\,\Delta\rho^2(p_1,p_2)\,V^2(p_1,p_2)\,R_g{}^2(p_1,p_2)\,\mathrm{d}p_1\,\mathrm{d}p_2}{\overline{\Delta\rho V^2}} \quad (9)$$

In eq 8 the denominator is just the average mass in the beam, the first term of which is the average mass per particle, $\overline{M} = \int\int f(p_1,p_2)\ M(p_1,p_2)\,\mathrm{d}p_1\,\mathrm{d}p_2$, and the second term, $N_0{}^{-1}N_LW_B(\Gamma^{-1} - \gamma^{-1})$, is the amount of bile salt free in solution. Here, N_0, N_L, and W_B are, respectively, the Avogadro constant, the average number of fatty lipid molecules per particle, and the gram molecular weight of the bile salt (see materials section). The molar ratio of lipid to bile salt bound in

the particle, γ^{-1}, is only slightly smaller than the bulk molar ratio; thus, the second term can usually be ignored. Finally, taking into account the resolution of the instrument $R(Q)$, the measured intensity is

$$I(Q) = \frac{R(Q) \otimes \overline{\langle P(Q) \rangle}}{\overline{M} + N_0^{-1}\overline{N_L} W_B(\Gamma^{-1} - \gamma^{-1})} \tag{10}$$

where $\otimes$ is the convolution operator. We calculated $R(Q)$ using standard methods.[34]

To calculate $S(Q)$ for charged particles, we use the rescaled mean spherical approximation (RMSA) to the solution of the charged particle interactions using one-component macro-ion theory[37] for dilute particle solutions.[38] In this, the charged particle interactions are described by the Yukawa interaction potential at a distance r,

$$U(r) = \frac{(ze)^2}{4\pi\epsilon\epsilon_0 R(1 + \kappa R)^2} \frac{\exp[-\kappa(r - 2R)]}{r} \tag{11}$$

where κ is the inverse Debye length, $\epsilon\epsilon_0$ is the permittivity, ze is the total particle charge, and R is the particle radius. Equation 11 is used to solve for the direct correlation function, $c(r)$, in the Ornstien−Zerneke equation for the total correlation function, $h(r)$,

$$h(r_{1,2}) = c(r_{1,2}) + \rho \int h(r_{2,3})\, c(r_{1,3})\, \mathrm{d}r_3 \tag{12}$$

subject to the closure relations,

$$c(r) = -\frac{U(r)}{k_b T}, \quad r > \mathrm{R}$$

$$g(r) = 0, \quad r < R \tag{13}$$

In eq 12 $r_{1,2}$ refers to the distance between two particles, and the integration is over all positions of a third particle, 3. In eq 13, k_b, is the Boltzman constant, T is the temperature, and g(r) is the particle pair probability distribution function, $g(r) = h(r) + 1$. The structure factor is calculated from the Fourier transform, $\hat{c}(Q)$, of c(r) as

$$S(Q) = [1 + 24\phi\, \hat{c}(Q,\phi)]^{-1} \tag{14}$$

Here, ϕ, is the volume fraction of particles.

The RMSA formalism in the limit of $z = 0$ becomes the closed-form solution of the Percus−Yevick equation for monodispersed hard spheres. For this case we use this solution directly,[39,40]

$$\hat{c}(Q,\phi) = \frac{a(\phi)}{x^3}[\sin(x) - x\cos(x)] + \frac{b(\phi)}{x^4}[2x\sin(x) - (2 - x)\cos(x) - 2] + \frac{c(\phi)}{(x)^6}\{-x^4\cos(x) + 4[(3x^2 - 6)\cos(x) + (x^3 - 6x)\sin(x) + 6]\} \tag{15}$$

with $x = 2QR$, $a(\phi) = (1 + 2\phi)^2/(1 - \phi)^4$, $b(\phi) = -6(1 + \phi/2)^2/(1 - \phi)^4$, and $c(\phi) = (\phi/2)(1 + 2\phi)^2/(1 - \phi)^4$.

For polydispersed and quasi-spherical systems we compute $S'(Q)$ in eq 3, using the procedure of Kotlarchyk and Chen:[36]

$$S'(Q) = 1 + \beta(Q)[S(Q) - 1] \tag{16}$$

where

$$\beta(Q) = \frac{|\overline{\langle F(Q) \rangle}|^2}{\overline{\langle |F(Q)|^2 \rangle}} \tag{17}$$

We model the mixed micelles as cylinders, as discussed above, in which case the spherical-averaged form factor is given by eq 1 and the spherical-averaged amplitude factor in eq 17 is given by

$$\langle F(Q) \rangle = 4\int_0^{2\pi} \frac{\sin(QH/2\cos\theta)}{QH\cos\theta} \frac{J_1(QR\sin\theta)}{QR\sin\theta} \sin\theta\, \mathrm{d}\theta \tag{18}$$

We require an equivalent spherical radius, R_{eq}, for use in the RMSA procedure, setting $R = R_{eq}$ (see eqs 11 and 13). We find that the best choice for R_{eq} is given by that for a sphere with the same radius of gyration of the cylinder,

$$R_{eq} = \left[\frac{5}{3}\left(\frac{R^2}{2} + \frac{H^2}{12}\right)\right]^{1/2} \tag{19}$$

rather than the equivalent particle volume or volume fraction.

Refinement of Models of Particle Interactions, Particle Size, Shape, and Polydispersity in the Mixed Micelles. The calculations of particle shape, size distribution, and $S'(Q)$ are clearly coupled. For mixed micelle samples, we devised an iterative procedure based on the decoupling approximation (eqs 3, 16, and 17). We started by using the estimates of the particle R_g and ΔM_0 from the Guinier and $D-L$ analyses (eqs 4 and 5). The volume and aggregation numbers of the mixed micelles were calculated from ΔM_0 and from the molecular volumes[17] of each component. To determine the aggregation numbers, we assumed that all of the fatty lipid (monoolein or oleate/oleic acid) was incorporated into particles. We assumed further that the amount of bile salt in the particles could be calculated from the difference between the total bile salt solution concentration and the intermicelle concentration (IMC). The IMC's have been determined for cholylglycine and chenodeoxycholylglycine in the presence of either EYPC[26] or monoolein,[41,42] and they cluster around 4 mM for cholylglycine and 1 mM for chenodeoxycholylglycine regardless of which fatty amphiphile is present. The mixed micelles were modeled as straight circular cylinders, and the values of R and H were calculated from the measured R_g and V. The cylinder height was calculated from a solution of

$$H^3 - 12R_g^2 H + \frac{6V}{\pi} = 0 \tag{20}$$

and the cylinder radius was calculated from

$$R = \left(\frac{V}{\pi H}\right)^{1/2} = \left(2R_g^2 - \frac{H^2}{6}\right)^{1/2} \tag{21}$$

These values were then used in the RMSA calculation, using the decoupling approximation, to give $S'(Q)$. $I(Q)$ was then calculated from the Guinier parameters and using eqs 1, 3, and 18. At this stage of the calculation, we adjusted the total particle charge to give the best fit. A new value of $\overline{\langle P(Q) \rangle}$ was then computed, using eq 3, by dividing the measured intensity by the $S'(Q)$ calculated above.

We use the new value of $\overline{\langle P(Q) \rangle}$ to characterize the polydispersity by calculating the PDF from eqs 10 and 7 using the maximum entropy algorithm, MEMSYS5, of Skilling and Gull.[43−45] The maximum entropy solutions for the PDF's are not unique. The MEMSYS5 package introduces an intrinsic correlation function (ICF) to allow for inclusion of a prior point-

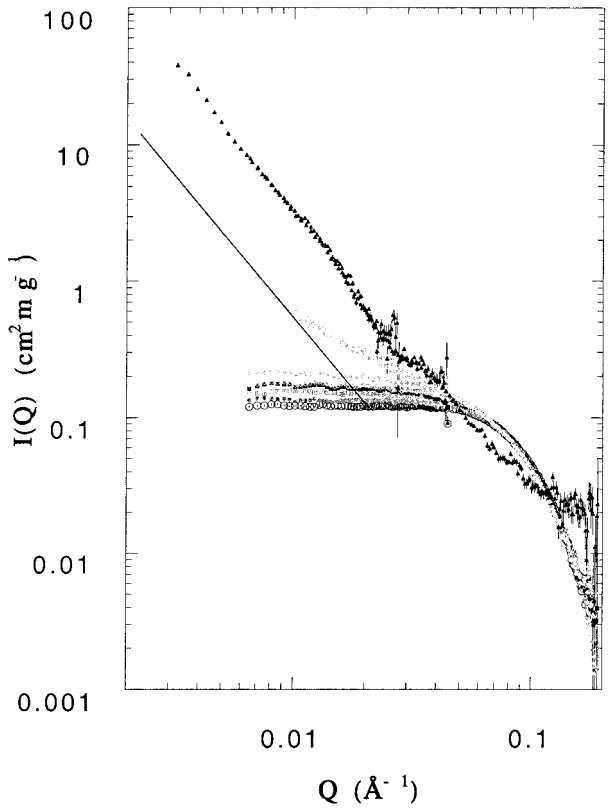

Figure 1. Scattering from mixtures of chenodeoxycholylglycine with monoolein and oleate/oleic acid: ○, 13.6 g/L; ●, 9.1 g/L; □, 6.0 g/L; ■, 4.5 g/L; ◇, 3.6 g/L; ◆, 2.3 g/L; △, 1.8 g/L; ▲, 0.45 g/L. The line shows the power law $I(Q) \propto Q^{-2}$.

to-point correlation.[46] We used a Swartz distribution or the ICF function, varying its parameters to generate the different solutions. We chose the PDF's fitting $\langle P(Q) \rangle$ with $\chi^2/(N) \approx 1$ (N is the number of data points) that had the smallest variance in each of the independent variables.

New estimates for R_g and ΔM_0 were then computed from the PDF's using eqs 8 and 9. These values were confirmed using the Guinier analysis (eq 5) of the $\langle P(Q) \rangle$. New values for the weighted cylinder heights and radii were calculated from the R_g and micelle volumes derived from ΔM_0 using eqs 20 and 21. Mean values of R and H were also calculated from the PDF's. Aggregation numbers were estimated from both the weighted and mean particle parameters, as described above. The calculation for $S'(Q)$ was then repeated using the weighted R and H and fixing the total micelle charge using the number-average aggregation numbers by assuming that all the bile salt and half the oleate is ionized at this pH. We then compared the fits of the models with the data. No additional iterations were performed if the fits were satisfactory ($\chi^2/N \cong 1$). Otherwise, the procedure was repeated.

Results

Mixtures of Chenodeoxycholylglycine with Monoolein and Na Oleate/Oleic Acid. Mixtures containing chenodeoxycholylglycine with monoolein and oleate/oleic acid were clear except for the most dilute sample (0.45 g/L total lipid), which was slightly turbid. The small-angle neutron scattering from these samples is shown in Figure 1.

In the range of total lipid concentrations between 13.6 and 2.3 g/L the scattering was characteristic of globular mixed micelle particles. The presence of repulsive interparticle interactions was evident, which tended to suppress the scattering intensity at low Q (eqs 3 and 16). The appearance of $D-L$ and Guinier plots (Figure 2) confirmed that there were significant repulsive particle interactions in the samples. Even so, the plots showed that valid Guinier regimes could be identified in the samples from 6.0 to 2.3 g/L. However, the values for R_g derived from the $D-L$ analysis (eq 4) were slightly larger by 3−8% than the values derived from Guinier analysis, indicating residual repulsing interactions. The positive deviation of α from the ideal value of zero (Table 1) was indicative of this as well. The differences in R_g tended to decrease with decreasing concentration, as expected (see eqs 5 and 6). At higher concentrations (13.6 and 9.1 g/L) a direct measure of R_g was not possible using the criterion that $R_gQ \leq 1.3$ (Figure 2). We extended the criterion to $R_gQ \leq 1.7$ (Table 1) to obtain an estimate for R_g and ΔM_0 for the next step in the analysis. We do not recommend such a procedure otherwise.

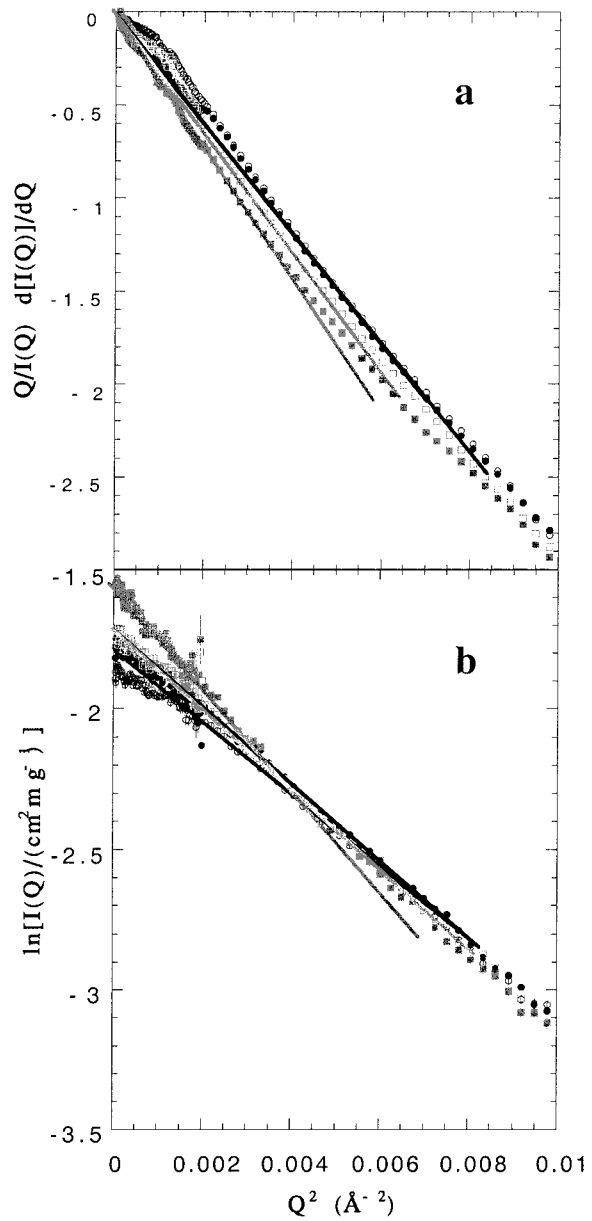

Figure 2. Derivative−log and Guinier analysis of data from mixtures of chenodeoxycholylglycine with monoolein and oleate/oleic acid: (a) derivative−log analysis; (b) Guinier analysis. Data: ○, 6.0 g/L; ●, 4.5 g/L; □, 3.6 g/L; ■, 2.3 g/L. Lines in parts a and b are fits to eqs 5 and 4, respectively.

TABLE 1: Guinier Analyses of Chenodeoxycholylglycine− and Cholylglycine−Monoolein−Oleate/Oleic Acid Mixtures

C_{lipid} (g/L)	α[a]	R_g [a] (Å)	ΔM_0 [b] (cm²/g)	R_g [b] (Å)
Chenodeoxycholylglycine−Monoolein−Oleate/Oleic Acid				
13.6	0.05(0.02)	20.7(0.1)[c]	164(2)[c]	19.6(0.1)[c]
9.1	0.05(0.01)	21.0(0.1)[c]	156(1)[c]	19.0(0.1)[c]
6.0	0.01(0.01)	21.1(0.1)	168(1)	19.6(0.1)
4.5	−0.02(0.02)	21.1(0.1)	177(1)	20.1(0.1)
3.6	−0.01(0.01)	21.9(0.1)	186(2)	21.2(0.1)
2.3	−0.02(0.01)	23.0(0.1)	211(1)	23.2(0.1)
Cholylglycine−Monoolein−Oleate/Oleic Acid				
15.7	0. 1(0.004)	20.1(0.1)[c]	129(1)[c]	*19.1(0.1)*[c]
10.5	0.05(0.02)	20.8(0.1)[c]	132(1)[c]	19.4(0.1)[c]
7.0	−0.01(0.02)	21.8(0.3)[c]	156(1)[c]	21.2(0.1)[c]
5.2	−0.4(0. 1)	315(13)	15400(200)	329(1)
4.2	−0.05(0.1)	315(12)	25300(200)	310(1)
2.6	0.04(0.07)	242(9)	27800(100)	232(1)

C_{lipid} (g/L)	α[a]	R_c[a] (Å)	Δm_0[b] (cm² Å^{-1} g^{-1})	R_c[b] (Å)
4.2	−1.01(0.01)	13.9(0.1)	2.2(0.1)	13.8(0.1)

C_{lipid} (g/L)	α[a]	R_d[a] (Å)	$\Delta\mu_0$[b] (cm² Å^{-2} g^{-1})	R_d[b] (Å)
2.6	−1.99(0.02)	7.1(0.1)	0.051(0.001)	7.0(0.1)
2.1	−1.98(0.01)	7.6(0.1)	0.051(0.002)	7.4(0.1)

[a] Estimated by fitting data to eq 5. The numbers in parentheses are the mean squared deviation estimated from the regression. [b] Calculated from the Guinier analysis (eq 4). The numbers in parentheses are the mean squared deviations estimated from the regression. [c] Values calculated using the Guinier analysis such that $R_gQ \leq 1.7$.

The values for R_g and ΔM_0 (Table 1) were used as the starting points for the analysis of $S'(Q)$ and polydispersity, using the methods described above. $I(Q)$ calculated from these parameters, but assuming monodispersed particles, agreed well with the experimental data over most of the measured Q domain (Figure 3a). Though apparently minor, there were discrepancies at higher Q (Figure 3a) in that the modeled $I(Q)$ consistently fell below the data. The discrepancies were taken to indicate polydispersity in R and/or H. Examples of the refined fits, taking polydispersity into account, are shown in Figure 3b. The model fit within the entire range of measured Q with the slight exception of the fit at low Q at the highest concentration, where the model fell below the data slightly. The joint PDF's in R and H derived from the maximum entropy calculation are shown as the marginal distributions in parts a and b of Figure 4, respectively. The estimates for the weighted values of particle ΔM_0, R_g, particle volume, H, and aggregation numbers are in Table 2. The mean values of R and H, the rms values of the PDF's, and the mean aggregation numbers are shown in Table 3. The structure-factor-corrected Guinier estimates of ΔM_0 and R_g (Table 2) tended to be between the initial Guinier and $D-L$-derived estimates (Table 1) of R_g. This behavior is consistent with the systematic errors anticipated in the determination of ΔM_0 and R_g when data are not corrected for repulsive interactions.

The values of R and H calculated from the new estimates of R_g and ΔM_0 (Table 3) emphasized a slightly elongated particle shape that increased slightly in length (aspect ratios, $\delta = H/(2R)$, increasing from 1.1 to 1.5) as the concentration decreased. On the other hand, the means and the modes of R and H showed almost globular particles with δ between 1.0 and 1.2 that did not change significantly with decreasing concentration (Figure 4; Table 3). In the 2.3 g/L sample, however, all maximum entropy solutions for the PDF had two modes. One mode ($H = 32$, $R = 23$ Å) corresponded to a disk or tabletlike micelle with δ of about 0.7. The other mode ($H = 76$, $R = 13$ Å) corresponded to an elongated micelle with δ of 2.9 (Table 3).

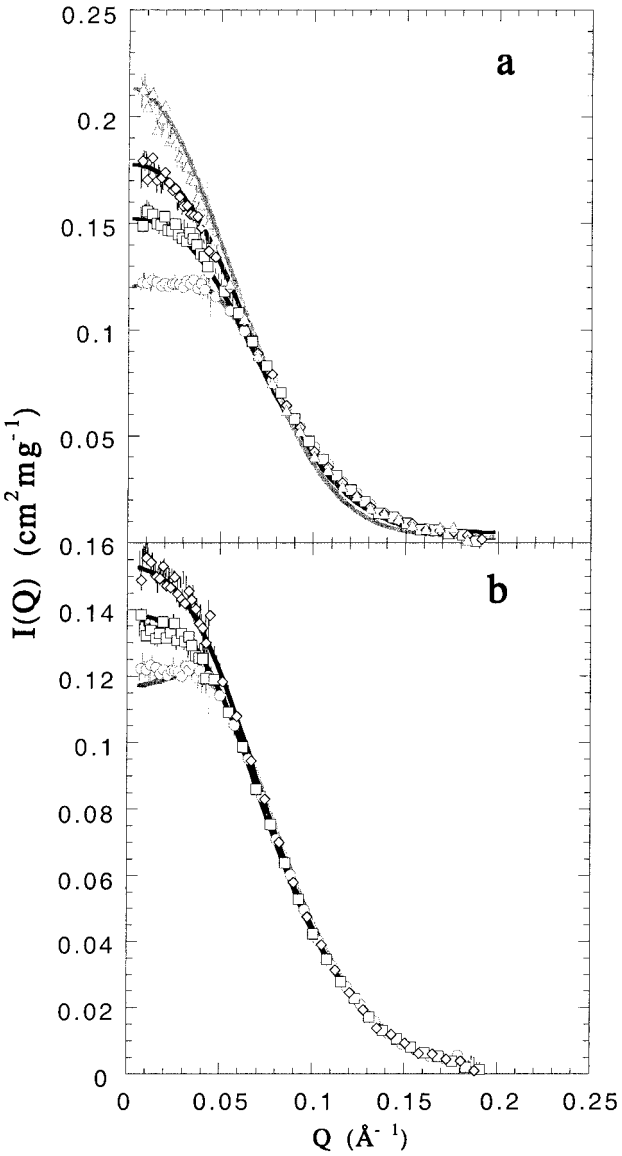

Figure 3. Scattering from solutions containing chenodeoxycholylglycine, monoolein and oleate/oleic acid, showing comparison with models. (a) Assuming monodispersed particles: ○, 13.6 g/L; □, 6.0 g/L; ◇, 3.6 g/L; △, 2.3 g/L. Lines are fits to eq 3, using the parameters in Table 2, as described in the text. (b) Data: ○, 13.6 g/L; □, 9.1 g/L; ◇, 6.0 g/L. In parts a and b every fifth data point is displayed for clarity. Lines in part b are fits calculated from the maximum entropy algorithm leading to the model parameters given in Tables 2 and 3, as described in the text. A representative sampling is shown in parts a and b.

The δ of the means was 1.5 (Table 3), a value similar to the weighted δ (Table 2). The polydispersity of the samples, as measured by the rms of the PDF, tends to increase with decreasing concentration for both R and H in all of the samples studied (Table 3). Because we model the mixed micelles as straight circular cylinders with constant $\bar{\rho}$, a deviation from this in the actual micelles will show up as apparent polydispersity in the PDF's.

At 1.8 g/L, the scattering changed substantially. There was an increase in the scattering intensity and a change in shape of the scattering curve, which followed $I = Q^{-2}$ over the lowest Q values (Figure 1). The higher-Q part of the scattering curve at this concentration, however, retained the appearance observed in the more concentrated solutions, suggesting the coexistence of particles with two different forms. One of the forms was

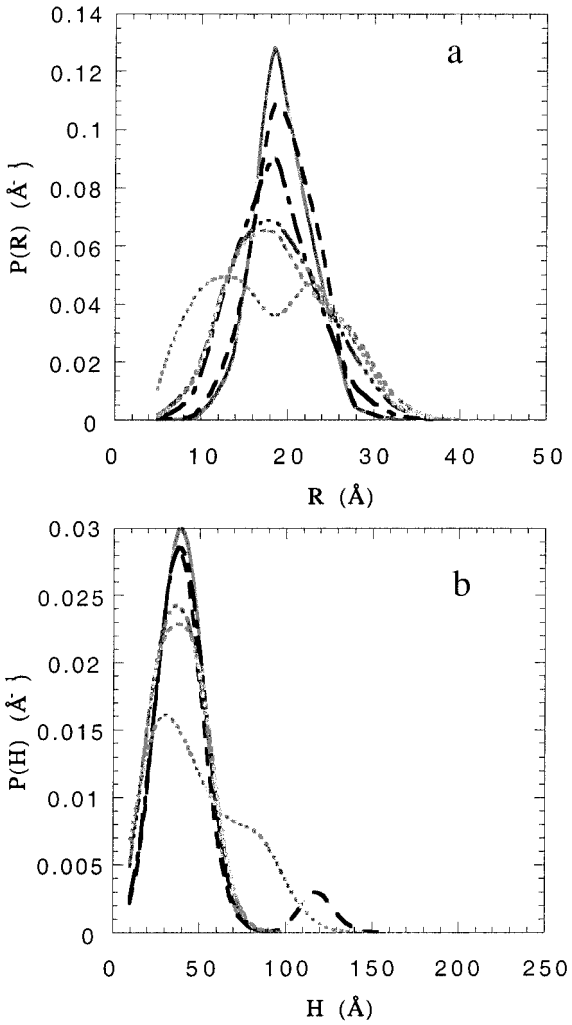

Figure 4. Marginal distributions for *R* and *H* for mixed micelles in solutions containing chenodeoxycholylglycine monoolein and oleate/oleic acid: (a) marginal distribution for *R*; (b) marginal distribution for *H*; (−) 13.6 g/L; − − −, 9.1 g/L; − - -, 6.0 g/L; − - - -, 4.5 g/L; − − −, 3.6 g/L; - - -, 2.3 g/L.

likely to be the mixed micellar phase. The phase transition to the phase giving the Q^{-2} dependence of the scattering, consistent with planar morphology, was complete when the sample was diluted to 0.45 g/L. The planar phase could consist of stacked ribbonlike lamellae or lamellae with elongated void defects, such as can be observed in mixtures of cholylglycine or cholyltaurine with EYPC at high pressure.[47,48]

Mixtures of Cholylglycine with Monoolein and Oleate/Oleic Acid. Mixtures of cholylglycine with monoolein and oleate/oleic acid were clear at concentrations of 15.7 to 7.0 g/L. Slight turbidity was observed in the samples containing 5.2 and 4.2 g/L lipid, but the samples were seen to be clear again when diluted to 2.6 g/L. Slight turbidity was again observed in the 2.1 g/L sample. The turbidity increased with further dilution. The scattering from these samples is shown in Figure 5.

The most concentrated samples in the series, 15.7 and 10.5 g/L, showed scattering characteristic of globular micelles with repulsive interactions. The *D*−*L* analysis showed that there were no valid Guinier regimes for these two samples. We again extended the analysis to $R_gQ \leq 1.7$ so that we could obtain the first estimates of R_g and ΔM_0 (Table 1) for calculating the full model.

Models the 15.7−7.0 g/L samples that did not include polydispersity gave lower $I(Q)$ than the data at high Q. The

TABLE 2: Particle Parameters for Mixed Micelles from Maximum Entropy Analysis

C_{lipid} (g/L)	ΔM_0 [a] ($cm^2\,g^{-1}$)	$\overline{R_g^2}^{1/2}$ [b] (Å)	$\overline{v^2}/v$ [c] ($Å^3$)	H [d] (Å)	R [e] (Å)	N_{BS} [f]	N_{MO} [g]	N_O [h]
Chenodeoxycholylglycine−Monoolein−Oleate/Oleic Acid								
13.6	166	19.8	62 100	46.3	20.7	48.3	20.1	40.1
9.1	170	21.3	64 300	57.5	18.9	49.1	21.1	42.2
6	175	20.5	67 350	49.4	20.8	50.0	22.6	45.3
4.5	187	21.3	73 200	53.0	21.0	52.7	25.2	50.4
3.6	191	21.7	76 125	54.7	21.0	53.0	26.9	53.7
2.3	214	23.6	89 700	62.9	21.3	55.8	34.1	68.1
Cholylglycine−Monoolein−Oleate/Oleic Acid								
15.7	130	20.4	56 300	55.2	18.0	44.7	17.9	35.7
10.5	146	21.9	66 000	60.6	18.6	48.8	22.3	44.5
7.0	160	22.5	77 400	60.1	20.2	49.7	28.8	57.7
Chenodeoxycholylglycine−Oleate/Oleic Acid								
16.7[i]	131	22.7	49 600	69.4	15.1	40.7		47.9
10[i]	131	21.2	50 200	62.0	16.1	40.5		49.3
6.6[j]	151	22.5	58 400	66.3	16.7	46.0		58.6
5[i]	140	21.9	55 350	64.1	16.6	42.6		56.8
4[j]	168	24.0	67 500	71.5	17.3	50.6		70.8
2.5[j]	210	27.4	86 000	83.6	18.4	60.5		99.6
Cholylglycine−Oleate/Oleic Acid								
16.7[j]	88.8	19.3	35 900	57.2	14.1	27.1		37.5
10.0[j]	78.9	19.9	33 750	60.8	13.3	23.1		37.9
6.6[i]	148	23.5	67 800	68.9	17.7	37.0		84.6
5.0[j]	183	28.0	89 300	86.2	18.2	40.1		124.3
5.0[i]	230	29.9	112 900	91.5	19.8	50.6		157.2
4.0[i]	373	37.3	197 300	116	23.3	56.0		311.8

[a] The micelle contrast factor, computed as $\Delta M_0 = \sum N_i b_i - V\rho_{D_2O}$. The sum is over the product of aggregation number and scattering length of all the micelle components *i*. [b] Statistical weight for the radius of gyration according to eq 9 computed from the PDF, $f(R,H)$. [c] Statistical weight for the volume according to eq 8 computed from the PDF, $f(R,H)$. [d] Cylinder height, calculated from the solution of eq 20. [e] Cylinder radius. Determined using eq 21. [f] Average micelle aggregation number of chenodeoxycholylglycine, calculated as $C_{mic}M_{CDCG}N_0/N$, where C_{mic} is the micellar molar concentration of bile salt and M_{CDCG} is the molecular weight. [g] Average micelle aggregation number of monoolein, calculated as $C_{mic}M_{MO}N_0/N$, where C_{mic} is the micellar molar concentration of monoolein, as described in the text, and M_{MO} is the molecular weight. [h] Average micelle aggregation number of oleic acid/Na oleate, calculated as $C_{mic}M_ON_0/N$, where C_{mic} is the micellar molar concentration of oleate, as described in the text, and M_O is the molecular weight. [i] Taken from the second dilution set (see Table 5). [j] Taken from the first dilution set (see Table 5).

micelle parameters that were calculated from the maximum entropy derived PDF's are shown in Tables 2 and 3. The fits of the refined model were within the deviation of the data over the entire measured Q domain. The final R_g and ΔM_0 values (Table 2) were higher than the initial estimates (Table 1), as anticipated, although the values for R_g were larger than both the Guinier and *D*−*L*-derived estimates. The *H* and *R* values computed from the Guinier parameters (Table 2) again emphasized particles with slightly elongated forms with δ in the range 1.5−1.6. On the other hand, the means and modes for the maximum entropy PDF's gave δ closer to 1.1 (Table 3). Over the limited concentration range accessible for these samples, there was an increase in the polydispersity of the PDF's for *R* and *H* with decreasing concentration (Table 2).

Samples at 7.0, 5.2, and 4.2 g/L, appeared to be in a coexistence regime of micelles and vesicles. The size of the particles contributing to the large increase in the low-Q part of the scattering curve at 7.0 g/L were too large to determine by these SANS measurements. A putative mixed micelle contribution to the 7.0 g/L sample was picked out by *D*−*L* analysis. The Guinier and mean *R* and *H* values (Tables 2 and 3) had $\delta = 1.6$, whereas δ calculated from the modes was 1.1. The *D*−*L*

TABLE 3: Probability Distribution Function Parameters from Maximum Entropy Analysis

	cylinder height, H (Å)			cylinder radius, R (Å)					
C_{lipid} (g/L)	mean	mode	rms	mean	mode	rms	N_{BS} [a]	N_{MO} [b]	N_O [c]
Chenodeoxycholylglycine−Monoolein−Oleate/Oleic Acid									
13.6	39.8	39	12.8	19.5	19	3.0	36.9	15.4	30.7
9.1	39.2	38	23.4	20.1	19	3.0	38.1	16.3	32.7
6.0	39.9	38	13.6	18.5	18	4.6	32.1	14.5	29.1
4.5	40.6	38	24.1	18.9	18	5.6	32.9	15.7	31.4
3.6	40.7	37	23.3	19.5	17	6.0	33.8	17.2	34.3
2.3	51.7	76	28.8	17.8	13[f]	7.1	32.0	19.5	39.1
		32			23				
Cholylglycine−Monolein−Oleate/Oleic Acid									
15.7	42.8	38	32.5	18.8	18	2.6	37.8	15.1	30.2
10.5	44.3	37	25.0	19.3	18	2.6	38.3	17.5	35.0
7.0	60.2	43	44.3	18.9	19	4.6	43.8	25.4	50.9
Chenodeoxycholylglycine−Oleate/Oleic Acid									
16.7[d]	46.3	38	19.0	19.2	18	3.8	44.0		51.8
10[d]	36.3	34	9.5	19.6	18	4.5	35.4		43.0
6.6[e]	48.7	54	16.9	20.9	18	4.7	52.7		67.1
5.0[d]	27.9	22	11.5	22.9	23	5.3	35.4		47.1
4.0[e]	35.2	28	15.9	22.2	23	7.3	40.8		57.1
2.5[e]	40.4	19	22.6	23.3	23	11.0	47.1		77.5
Cholylglycine−Oleate/Oleic Acid									
16.7[d]	27.2	23	11.5	19.8	18	3.5	25.4		35.1
10.0[d]	27.2	25	9.7	22.0	23	3.9	28.3		46.6
6.6[e]	40.4	47[f]	18.2	20.0	15[f]	7.9	30.6		66.4
		25			27				
5.0[e]	60.8	90[f]	34.4	20.6	10[f]	10.9	36.3		112.6
		21			32				
5.0[d]	36.5	80[f]	20.2	28.3	20[f]	12.1	41.1		127
		22			43				
4.0[e]	58.2	115[f]	45.6	31.6	14[f]	18.1	70.4		392
		18			52				

[a] Average micelle aggregation number of chenodeoxycholylglycine or cholylglycine, calculated as $C_{mic}MN_0/N$. Here, C_{mic} is the micellar molar concentration of bile salt, M is the molecular weight, and N is the number of micelles. [b] Average micelle aggregation number of monoolein. [c] Average micelle aggregation number of oleic acid/Na oleate. [d] Value taken from the second dilution set (see Table 5). [e] Value taken from the first dilution set (see Table 5). [f] Two modes were observed in the calculated PDF's from these samples, as described in the text. Values of H and R in the same row are the pairs that define each mode.

analyses (Figure 6a) of samples at 5.2 and 4.2 g/L also showed the presence of particles with two very different sizes. The larger particles present in these mixtures could be characterized by $D-L$ and Guinier analysis (Figure 7 and Table 1) giving R_g of about 315 Å for both samples. Data in the middle Q-domain $D-L$ analyses were extrapolated to $\alpha \cong 1$ at $Q = 0$ (Figure 6a), suggesting the presence of elongated or rodlike particles. The R_c of the putative elongated or rodlike micelles for the 4.2 g/L sample was 13.8−13.9 Å (Figure 6 and Table 1). This value for R_c (Table 1) corresponds to a radius of 19.7 Å, a value consistent with the R values given in Tables 2 and 3. There was no valid rodlike Guinier regime[49] for the 5.2 sample (Figure 6).

The scattering from samples in the range 2.6−2.1 g/L was characteristic of vesicles. In the higher Q domain, the $D-L$ analysis (Figure 8a) identified a region with $\alpha = 2$ (Table 1), indicating the local planar signature of a vesicle form factor. Both the Guinier and $D-L$ (Figure 8 and Table 1) analyses gave R_d between 7.0 and 7.6 Å, corresponding to a uniform SLV bilayer thickness of 24−26 Å. The overall Guinier radius (Figure 7 and Table 1) was found to be about 232 Å for the 2.6 g/L sample. By use of the relation[17]

$$R \cong \frac{R_d}{4\sqrt{3}} + \sqrt{R_g^2 - (1/8)R_d^2}$$

the Guinier analysis gave $R \approx 230$ Å. Maximum entropy analysis (a Gaussian was used as the ICF) was used to calculate a PDF for the 2.6 g/L sample. The value of R_g (Table 4) calculated from this PDF was in good agreement with the value determined from the Guinier analysis (Table 1). The mean values of R and t (Table 4) were lower than the values derived from R_g, as expected for polydispersed systems. Because the models assume uniform $\bar{\rho}$ within the vesicle wall, it is not possible to discriminate between true polydispersity in SLV bilayer thickness and smooth variations in $\rho(r)$ across the SLV bilayer. The same was true for discriminating between polydispersity in SLV size and the SLV's having deviations from spherical shape.

At the lowest concentrations studied, 0.52 and 0.39 g/L, the low-Q part followed a power law, $I(Q) \propto Q^{-4}$ (Figure 5b), crossing over to $I(Q) \propto Q^{-3}$ (Figure 5b) at larger Q, consistent with the presence of large structural domains of stacked lamellae.[47,48]

Mixtures of Cholylglycine or Chenodeoxycholylglycine with Oleate/Oleic Acid. The solutions containing chenodeoxycholylglycine−oleate/oleic acid were clear at higher concentrations but were turbid at and below 2.0 g/L. The scattering observed from the chenodeoxycholylglycine samples is shown in Figure 9.

The SANS data suggested globular mixed micelles between 16.7 and 2.5 g/L. The initial assessment of particle size and shape by $D-L$ and Guinier analysis is shown in Table 5. Again, we extended the Guinier analysis to $QR_g < 1.7$ for the sample at 16.7 g/L, which showed no valid Guinier domain due to repulsive particle interactions at the lowest Q values. The initial estimates from the $D-L$ analysis were larger than the Guinier

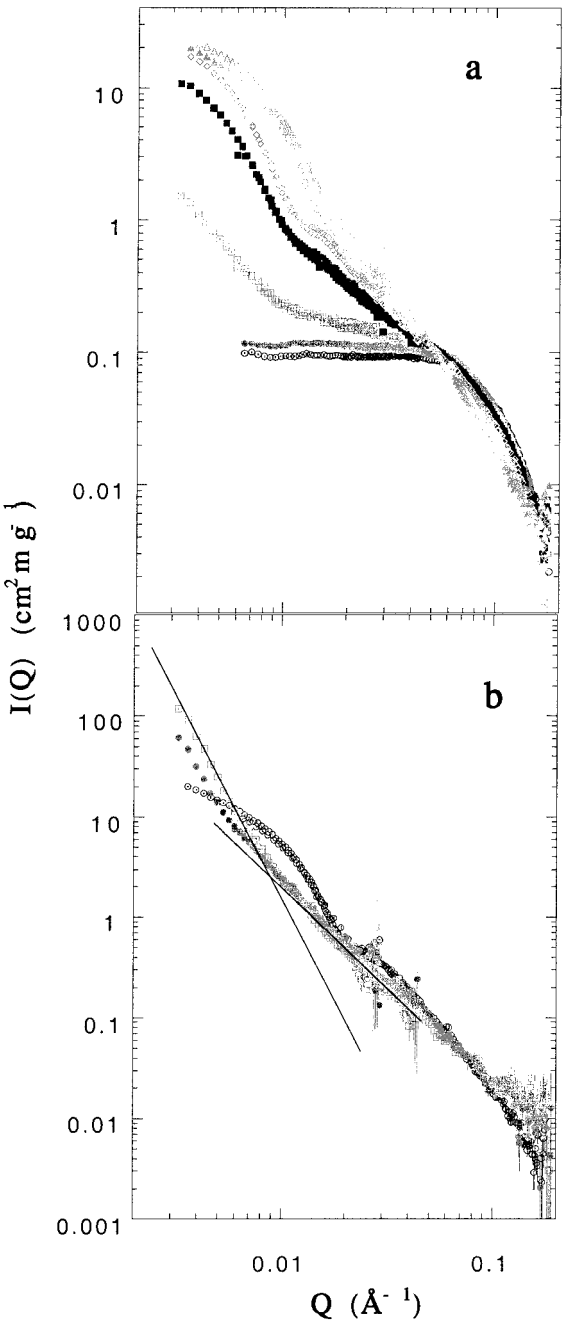

Figure 5. Scattering from mixtures of cholylglycine with monoolein and oleate/oleic acid. (a) Data: ○, 15.7 g/L; ●, 10.5 g/L; □, 7.0 g/L; ■, 5.2 g/L; ◇, 4.2 g/L; ◆, 2.6 g/L; △, 2.1 g/L. (b) Data: ○, 2.1 g/L; ●, 0.52 g/L; □, 0.39 g/L. In part b the lines at low and intermediate Q values correspond to power law scattering of $I(Q) \propto Q^{-4}$ and $I(Q) \propto Q^{-3}$, respectively.

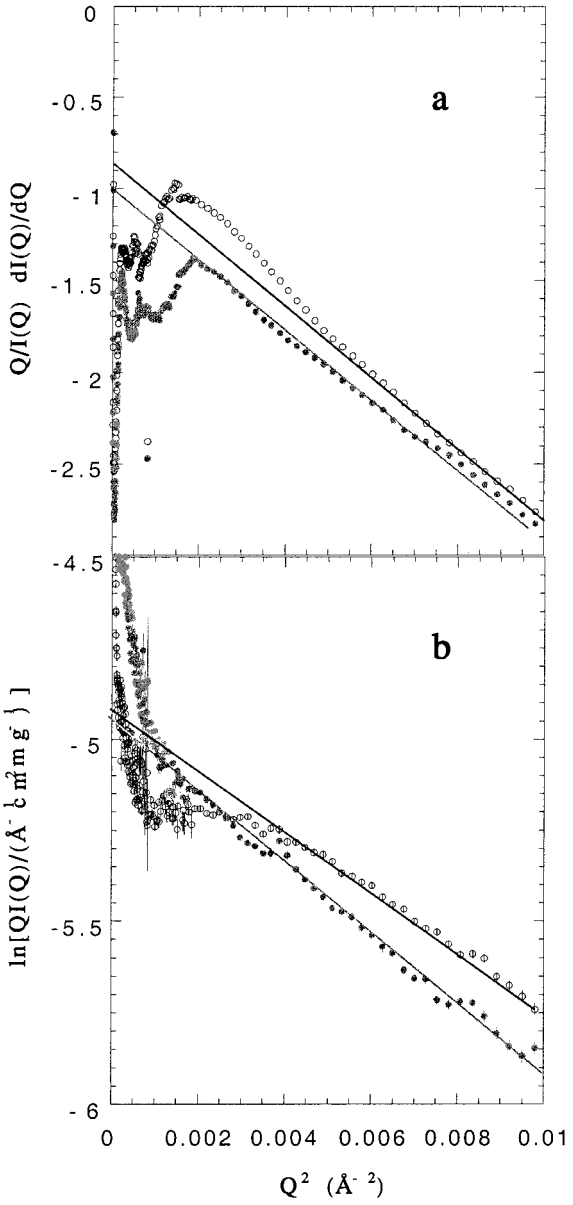

Figure 6. *D*−*L* and Guinier analysis of data from mixtures of cholylglycine with monoolein and oleate/oleic acid: (a) derivative−log analysis; (b) Guinier analysis for rodlike forms. Data in parts a and b: ○, 5.2 g/L; ●, 4.2 g/L. Lines in parts a and b are fits to eqs 5 and 4 (for $\alpha = 1$), respectively.

analysis, as expected. Without the inclusion of polydispersity, the values for $I(Q)$ computed using eq 3 were in agreement with the data at low Q but fell above the data at higher Q. With the calculation of $\langle P(Q) \rangle$, including polydispersity, the data and model agree (Figure 10). The refinements on the estimates for the Guinier parameters are given in Table 2. As expected, the refined values of R_g were between those estimated from the *D*−*L* and Guinier analyses (Table 5), and the refined ΔM_0 was larger than the initial estimate. For both parameters the differences between the refined and initial estimates correlated directly with the concentration.

The R and H values from the mixed micelle Guinier parameters (Table 2) suggested elongated micelles with an aspect ratio of about 2. The mean and mode values for the PDF's (Table 3) indicated more globular and even disklike micelles. The mean $H/(2R)$ was about 1 at higher concentrations and tended to decrease to smaller values with decreasing concentration. The modes showed a transition in aspect ratio from about 1.0 to 0.5 between 6.6 and 5.0 g/L. As in the previous two samples, the rms of the PDF increased with sample dilution (Table 3).

There was a transition to a large domainlike structure with an apparent coexistence between this phase and the globular mixed micelles at 2.5 g/L.

The scattering from the cholylglycine mixtures with oleate and oleic acid (Figure 11) indicated interacting globular micelles at the highest concentrations. The initial size and shape assessment from the *D*−*L* and Guinier analyses (Figure 12) indicated that there are mixed micelles present in the highest concentrations of cholylglycine and oleate/oleic acid (Table 5). There was no identifiable Guinier region for particles found in

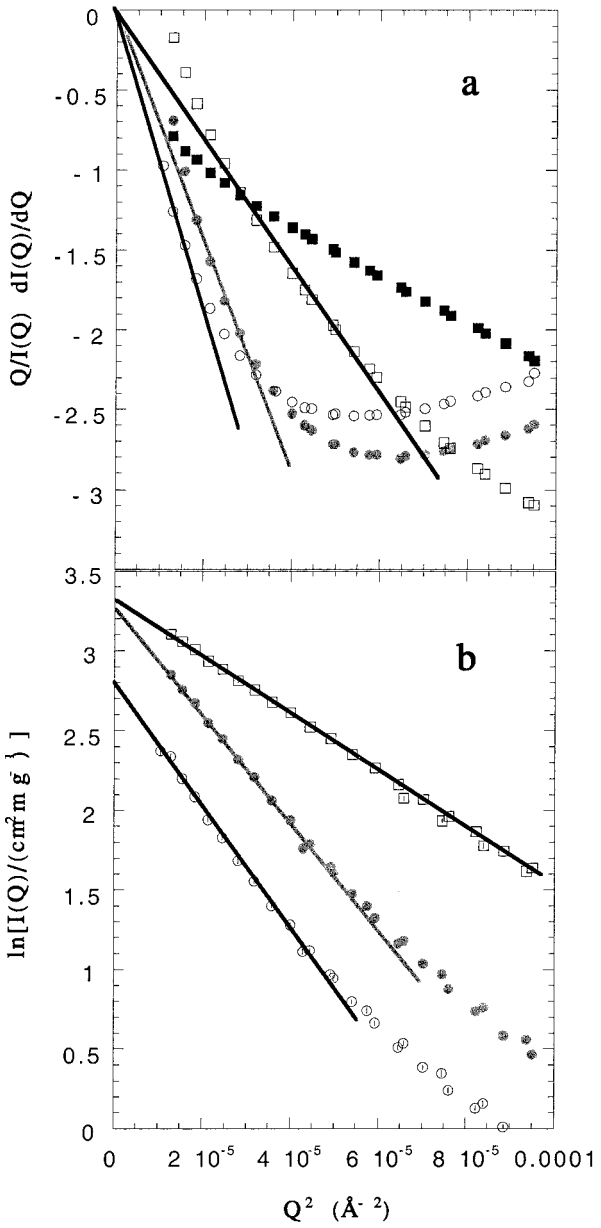

Figure 7. *D*−*L* and Guinier analysis of data from mixtures of cholylglycine with monoolein and oleate/oleic acid: (a) derivative−log analysis; (b) Guinier analysis. Data in part a: ○, 5.2 g/L; ●, 4.2 g/L; □, 2.6 g/L; ■, 2.1 g/L. Data in part b: ○, 5.2 g/L; ●, 4.2 g/L; □, 2.6 g/L. Lines in parts a and b are fits to eqs 5 and 4 (for $\alpha = 0$), respectively.

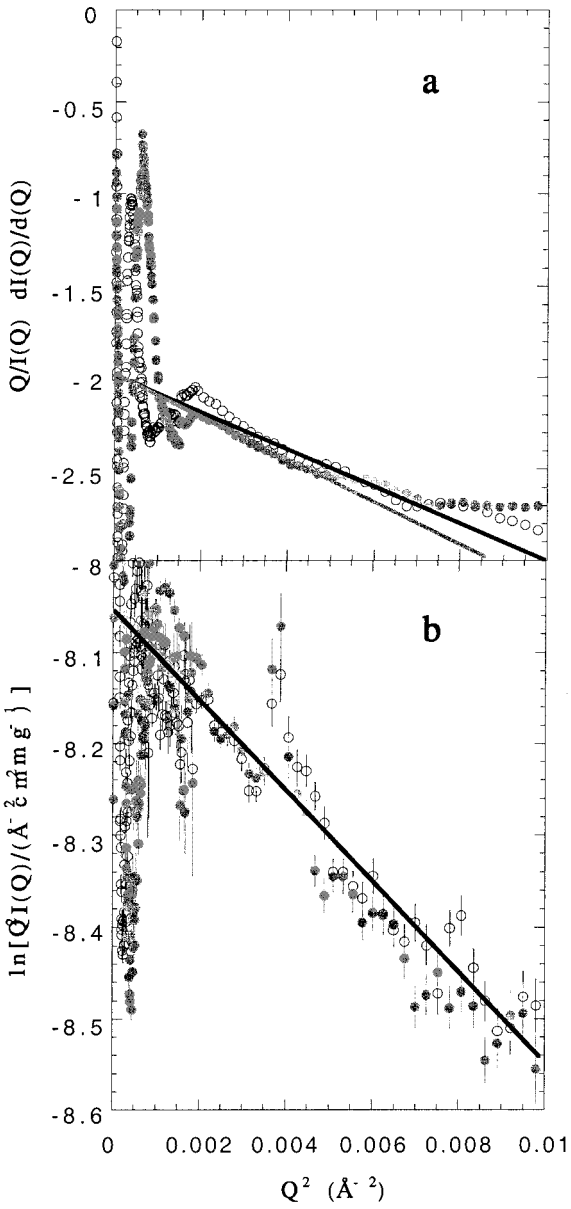

Figure 8. *D*−*L* and Guinier analysis of data from mixtures of cholylglycine with monoolein and oleate/oleic acid: (a) derivative−log analysis; (b) Guinier analysis for sheetlike forms. Data in parts a and b: ○, 2.6 g/L; ●, 2.2 g/L. Lines in parts a and b are fits to eqs 5 and 4 (for $\alpha = 2$), respectively.

the 16.7 and 10.0 g/L samples (parts a and b of Figure 12). Again, in these two cases we used an extended Guinier criterion to obtain initial estimates for R_g (Table 5).

We refined the analysis in the mixed micelle samples by including particle interactions and polydispersity. As with the other mixtures, we found that both were required to give good agreement between the data and the model over the measured Q domain. The R_g values computed from the PDF's (Table 2) were between those determined from the *D*−*L* and Guinier analysis. The refined ΔM_0 values tended to be larger than the initial estimates. The R and H values computed from the Guinier parameters (Table 2) emphasized elongated particles in the population and indicated aspect ratios of 2 and above. In contrast to this, the mean and mode values of the PDF's (Table 3) showed a different picture. At high lipid concentrations, the micelles in the cholylglycine−oleate/oleic acid mixtures were predominantly disklike with δ about 0.5−0.6 (Table 3). However, at concentrations from 6.6 to 4.0 g/L, two distinct particle populations became apparent as two modes in the PDF. One was disklike, the radius of which grew with decreasing concentration. The other population consists of elongated micelles that grew longer with decreasing concentration (Table 3).

There is evidence of a coexistence region consisting of large and possibly rodlike or elongated forms in the 4.0 g/L sample, as indicated by a region in the scattering where $\alpha \approx 1$ (Figure 12a). However, there was not a valid Guinier region that could be identified to measure the putative rod parameters. The interpretation of scattering data from samples at 2.5 and 2.0 g/L, although indicating sheetlike structures, was ambiguous, since we could not access sufficiently low Q to measure a Guinier radius. The *D*−*L* and Guinier analyses indicated (Figure 12 and Table 5) that the sheets have thickness similar to that of the cholylglycine−monoolein−oleate/oleic acid mixtures (Table

TABLE 4: Statistical Parameters of Probability Density Functions of Mixed Vesicles of Cholylglycine−Monoolein−Oleate/Oleic Acid

	vesicle radius, R		vesicle thickness, t			
C_{lipid} (g/L)	mean (Å)	rms (Å)	mean (Å)	rms (Å)	$\overline{v^2}/\overline{v}$ [a] (Å^3)	$\overline{R_{g_z}^2}^{1/2}$ [b] (Å)
2.6	206	47.9	17.1	2.8	1.1×10^7	245

[a] Statistical weight for volume according to eq 8 computed from the PDF, $f(R,t)$. [b] Statistical weight for the radius of gyration according to eq 9 computed from the PDF, $f(R,t)$.

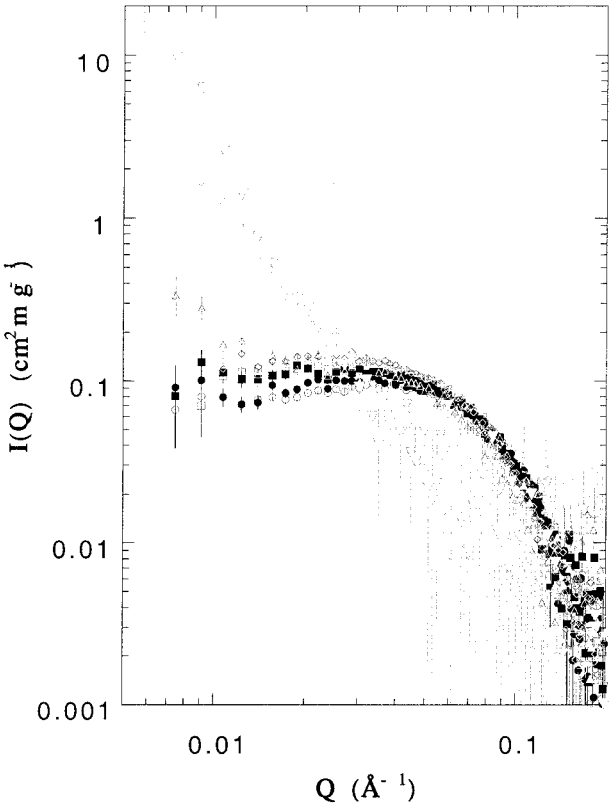

Figure 9. Neutron scattering data from chenodeoxycholylglycine oleate mixtures: ○, 16.7 g/L; ●, 10.0 g/L; □, 6.6 g/L; ■, 5.0 g/L; ◇, 4.0 g/L; ◆, 2.5 g/L; △, 2.0 g/L; ▲, 1.0 g/L, ▽, 0.375 g/L.

1). If these structures were vesicles, the maximum entropy analysis suggested that they have an average radius of 130 Å, with about 10% (rms) polydispersity, and a thickness of 37 Å with rms equal to 7 Å. These were mixed with much larger structures. However, an alternative model, assuming coexistence of elongated mixed micelles with large sheetlike structures, perhaps vesicles, with average size of 500 Å, explained these data equally well. There is a second transition to large domainlike structures between 2.0 and 1.0 g/L (Figure 11).

Discussion

Modeling Particle Interactions. A nontrivial issue in understanding self-assembling systems is the analysis of particle interactions. This is particularly important in the particles studied here, which have substantial charge at near neutral pH values. Progress has been made in the interpretation of scattering data to analyze particle interactions. These analyses include exact solutions and approximations for hard sphere interactions,[36,39,40] charged particle interactions,[37,38] and sticky (attractive) interactions.[50,51] In work on charged particle interactions, the particle charge, size, and shape were inferred from measurements of changes in scattering with concentration at sufficiently high concentrations where a correlation peak was observed.[37,38,51,52] It was assumed that the particle structure was independent of concentration over the range used. Recent work addressed the issue of electrostatic interaction in dilute solutions of symmetric cationic−anionic systems,[2,3] using the methods for charged particle interactions.[37,38] Other workers[5,24] have addressed the problem in the bile salt−EYPC systems by treating the interactions in the dilute limit using measurement of a second virial coefficient from light scattering. The interactions of wormlike micelles in the dilute to semidilute range have been treated, taking into account the second virial coefficient and entanglement effects in analogy to wormlike polymers.[7,53] These treatments, however, took into account only hard particle interactions. This was appropriate for the case of reverse micelles of soybean PC in isooctane,[53] but charge effects are likely to be important in the mixtures containing conjugated bile salt−EYPC aqueous micelles.[7] In addition to dealing with charged particle interactions, there are other assumptions used in previous work that do not apply to the mixtures studied here: the particle morphologies are highly sensitive to concentration, and we are working in a concentration regime where a correlation peak is not readily observable. In our earlier studies on monoolein, EYPC and DPPC with bile salts,[1,14−19] we ignored the effects of particle interactions, which were masked by dilution-induced particle growth, except at the high concentrations. Such effects could not be ignored in this study. Thus, for this work we devised an iterative method based on the RMSA method (eq 11−14) and the decoupling approximation (eqs 3, 16, 17) to separate scattering from particle shape, including polydispersity,

TABLE 5: Guinier Analyses of Chenodeoxycholylglycine− and Cholylglycine−Oleate/Oleic Acid Mixtures

C_{lipid} (g/L)	α [a]	R_g [a] (Å)	ΔM_0 [b] (cm^2/g)	R_g [b] (Å)
Chenodeoxycholylglycine−Oleate/Oleic Acid				
16.7[c]	0.02(0.02)	21.8(0.1)	126(2)[e]	21.3(0.2)
16.7[d]	−0.06(0.03)	20.6(0.8)	123(4)[e]	19.4(0.6)
10.0[c]	−0.01(0.01)	22.6(0.2)	146(3)	21.8(0.3)
10.0[d]	0.17(0.03)	22.5(0.2)	119(2)	19.1(0.5)
6.6[c]	0.00(0.01)	22.7(0.1)	144(1)	21.5(0.2)
5.0[d]	−0.04(0.03)	22.0(0.2)	136(2)	21.0(0.4)
4.0[c]	0.01(0.02)	24.5(0.6)	165(2)	23.2(0.3)
2.5[c]	−0.04(0.02)	28.3(0.2)	208(3)	26.7(0.5)
2.0[d]	−0.05(0.02)	24.3(0.2)	153(6)	24.9(0.9)
Cholylglycine−Oleate/Oleic Acid				
16.7[c]	0.03(0.02)	20.1(0.1)[e]	91(3)[e]	19.2(0.4)[e]
10.0[c]	0.02(0.02)	21.2(0.1)[e]	71(2)[e]	19.4(0.6)[e]
6.6[d]	−0.02(0.01)	23.6(0.1)	145(2)	23.0(0.3)
5.0[c]	−0.04(0.02)	28.1(0.2)	179(4)	27.2(0.8)
5.0[d]	−0.01(0.01)	30.7(0.2)	238(5)	30.7(0.6)
4.0[d]	−0.05(0.05)	39(1)	364(7)	36.4(0.8)

C_{lipid} (g/L)	α [a]	R_d [a] (Å)	$\Delta\mu_0$ [b] (cm^2 Å^{-2} g^{-1})	R_d [b] (Å)
2.5	−2.04(0.03)	7.3(0.3)	0.110(0.003)	8.6(0.5)
2.0	−2.06(0.04)	7.4(0.4)	0.085(0.004)	8.1(0.9)

[a] Estimated by fitting data to eq 5. The numbers in parentheses are the mean squared deviation estimated from the regression. [b] Calculated from the Guinier analysis (eq 4). The numbers in parentheses are the mean squared deviations estimated from the regression. [c] Values from first dilution set. [d] Values from second dilution set. [e] Values calculated using the Guinier analysis such that $R_gQ \leq 1.7$.

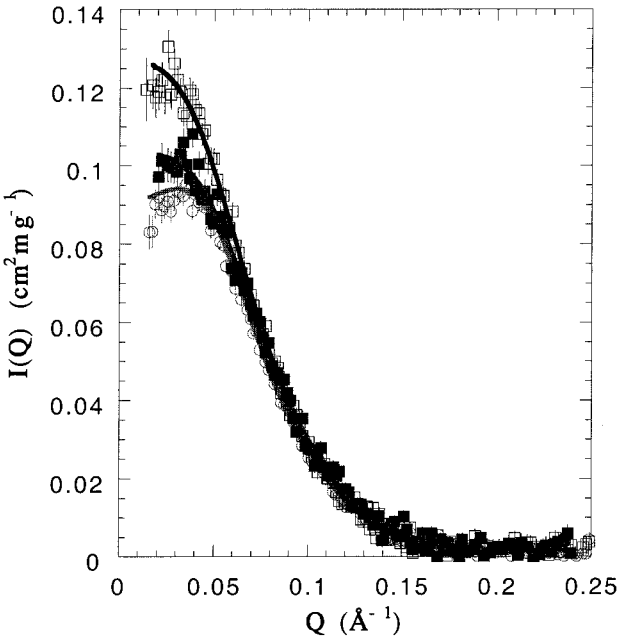

Figure 10. Scattering from solutions containing chenodeoxycholylglycine and oleate/oleic acid, showing comparison with models: ○, 16.7 g/L; ■, 10.0 g/L; □, 6.6 g/L. Lines are fits calculated from the maximum entropy algorithm leading to the model parameters given in Tables 2 and 3, as described in the text.

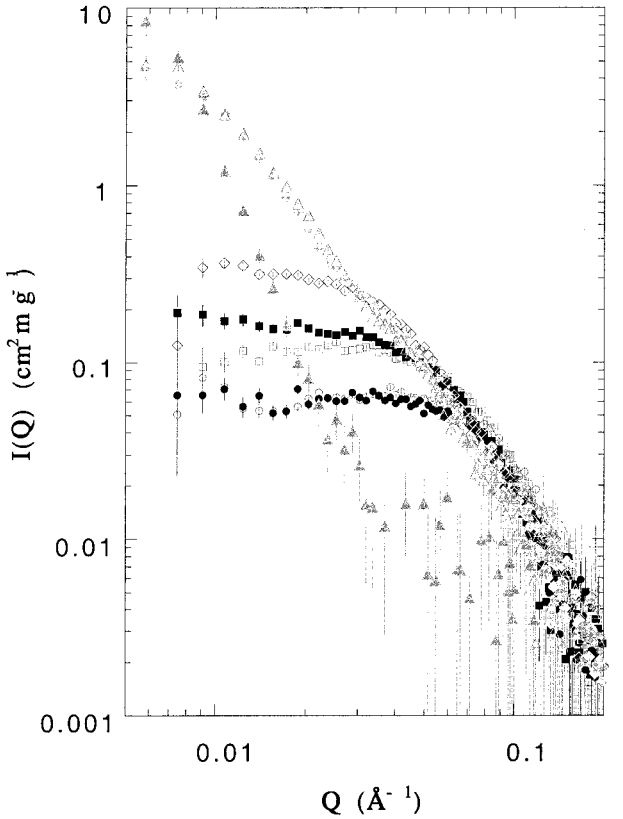

Figure 11. Neutron scattering data from cholylglycine oleate/oleic acid mixtures: ○, 16.7 g/L; ●, 10.0 g/L; □, 6.6 g/L; ■, 5.0 g/L; ◇, 4.0 g/L; ◆, 2.5 g/L; △, 2.0 g/L; ▲, 1.0 g/L.

and interactions that is usable over the intermediate concentration range used in this study.

There were satisfactory fits to the data when the RMSA parameters for the equivalent radius, R_{eq}, and average particle charge, $\bar{z}$ (eq 11), were calculated from R_g (eq 19) and the

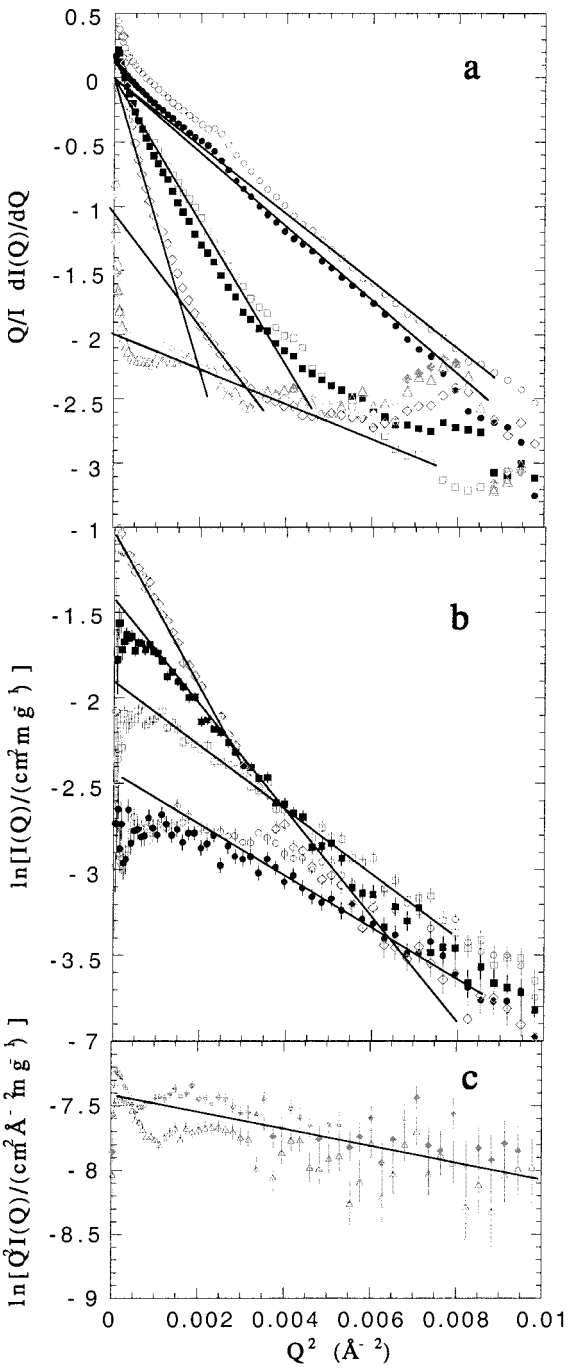

Figure 12. *D*−*L* and Guinier analysis of data from mixtures of cholylglycine with oleate/oleic acid: (a) derivative−log analysis; (b) Guinier analysis; (c) Guinier analysis modified for sheets. Data in parts a−c: ○, 16.7 g/L; ●, 10.0 g/L; □, 6.6 g/L; ■, 5.0 g/L; ◇, 4.0 g/L; ◆, 2.5 g/L; △, 2.0 g/L. Lines in part a are fits to eq 5. Lines in part b are fits to eq 4 for $\alpha = 0$, and lines in part c are for $\alpha = 2$ for 2.5 and 2.0 g/L.

mean particle aggregation, respectively. Average particle charge was calculated from the fraction of ionized group for each chemical species that buffer pH. These values were 1.0 for the conjugated bile salts and 0.5 for oleate. That the curves fit the data well using this gross assumption provides another observation on the complex issue of bound counterions in micelles. However, at these volume fractions, the fit at low Q is not extremely sensitive to the value of z chosen between $\bar{z} \pm 5$. The ratio of the effective charge on the particles to the total ionizable groups is 0.75. This value is significantly larger than

found for symmetric cationic−anionic systems of zero to one-half.[2] As expected, the refined values for R_g were between those estimated from the $D-L$ and Guinier methods without taking particle interactions into account (Tables 1, 2, and 5). Likewise, the refined values for ΔM_0 were larger than those calculated from the Guinier analysis. The differences between the Guinier parameters with and without correction for interactions were as large as 3%.

Comparison between the Bile Salt−Monoolein−Oleate/Oleic Acid and Bile Salt−Oleate/Oleic Acid Systems with Other Bile Salt−Fatty Amphiphile Mixtures. We have studied the effects of the negatively charged single-tailed surfactant, oleate, on the micelles and other particles formed in aqueous solution with conjugated bile salts. These characteristics, chosen to probe the effects of fatty lipid architecture and charge, are in contrast with those of the fatty lipids studied previously. The molar proportions of hydrocarbon chains to bile salt molecules were similar to those used previously with monoolein[17] and with some of the measurements using EYPC:[19] $\Gamma \cong 1.0$ for cholylglycine and $\Gamma \cong 1.2$ for chenodeoxycholylglycine.

In our work using monoolein as the fatty lipid,[17−19] we noted similarities in particle morphology between the monoolein-containing and phosphatidylcholine-containing colloids. In both systems, globular micelles, approximately 25−30 Å in radius, were present at the highest concentrations. This characteristic was also observed in all the mixtures studied here.

In all the systems studied previously, bile salts with EYPC, DPPC, or monoolein, the mixed micelles elongated on dilution. The radii of the particles did not change. The scattering data from the mixed micelle population of these samples were satisfactorily modeled assuming that the most significant contribution to polydispersity was variation in particle length.[15,17−19] In this study, however, the analysis of polydispersity in the mixed micelle phases revealed that different statistical measures of the micelle populations give different pictures of mixed micelle size and shape. The weighted averages of the PDF for R and H (Table 2) tended to emphasize the elongated particles in the population and indicated a small to moderate increase in particle length as the solutions were diluted. In contrast, the mean and mode values of the PDF's for R and H emphasized more spheroid particles in the population (Table 3), particularly when the samples contained both monoolein and oleate/oleic acid. The situation proved to be more complex for samples containing only oleate/oleic acid as the fatty lipid. For the chenodeoxycholylglycine samples, the mean and modes of the PDF suggested tabletlike micelles below 6.6 g/L total lipid concentration. For the samples with cholylglycine, the PDF's suggested elongated particles that coexisted with tabletlike mixed micelles below 10 g/L—a unique attribute among these systems. With dilution, the disklike micelles increased in radius and the elongated micelles increased in length. Because H and R are of similar size, there was some ambiguity in the analysis of polydispersity of these systems, since there was not clear separation in Q in the scattering from these parameters. This was unlike the cases studied earlier, where H was often considerably larger than R.

In solutions containing trihydroxy bile salts with either EYPC[1,14−15] or DPPC[16] the elongated particles became long rods with sufficient dilution. Similar growth of elongated particles was observed in EYPC mixtures with the dihydroxy bile salts,[5,6] but there is disagreement on this point.[24] In the present study, there was also evidence of elongation to form long rods in the cholylglycine−monoolein−oleate/oleic acid mixtures (Figure 6 and Table 1). This evidence, like that for the presence of long rods solutions containing monoolein,[17−19] is not strong, however. In both cases the possible existence of rods in sufficiently dilute solutions of cholylglycine monoolein and oleate/oleic acid was detected by the $D-L$ and Guinier analyses (Figure 6 and Table 1). This evidence was not as strong in any of the systems containing EYPC or DPPC, which showed the well-defined scattering signature of a rodlike particle. Indeed, a recent cryo-TEM study of cholate with monoolein in 0.15 mM NaCl failed to show long rodlike forms.[10] Cryo-TEM images of solutions with either bile salt or octylglucoside with EYPC readily showed rodlike micelles, on the other hand.[31,32] Thus, in the absence of confirming evidence, we must qualify our conclusion that long rods exist in systems containing monoolein or monoolein with oleate/oleic acids. The evidence was even weaker with the solutions containing cholylglycine and oleate/oleic acid. These solutions showed only a small, non-Guinier region that suggested the presence of rods (parts a and b of Figure 12).

The data presented in this study for the mixed micelles are consistent with the radial shell model proposed for elongated and rodlike mixed micelles of bile salts with EYPC, DPPC, or monoolein.[5,7,16−19,24,25,54] This model, first proposed by Nichols and Ozarowski,[54] has the cylindrical mixed micelle with the fatty lipid inserted perpendicular to the cylinder axis. In this model the fatty amphiphile is arranged radially in the rod.[6,7,16−19,24,25,32] The bile salts act as wedges between the fatty lipids. They also form the caps at the ends of the micelle. Taking into account the additional data from this work, the measured cylinder radii have a decreasing trend in the series phosphatidylcholine, monoolein, monoolein, and oleate.[1,6,7,14−19,24,25] The series is in the order of longest to shortest average length of the amphiphile, lending support to this model. Therefore, there was a common mode of self-assembly of mixed micelles in these systems, although there were important differences in behavior in the more dilute solutions. These studies support the hypothesis that the bile particle structure is conserved when triglyceride hydrolysis products replace phosphatidylcholine.

Modeling of Mixed Micelle Growth. The relatively insoluble fatty lipids may mediate the interactions that are necessary to promote growth by elongation, which we have proposed to occur by end-to-end fusion of mixed micelles.[17−19] According to this model, the bile salt inserted between the fatty lipid is energetically more favorable than that in the end caps. Hence, removal of the conjugated bile salts by mass action on dilution would be preferentially at the end caps. This mass action mechanism explains why the less soluble dihdroxy bile salts must be at lower concentrations for the mixed micelles to form long rods[5,6] (if long rods are present at all[24]) than the more soluble trihydroxy bile salts. The resulting "stickiness" (a consequence of the hydrophobic effect) of the exposed fatty lipid tails would promote micelle growth. This attractive potential is countered by the presence of an additional repulsive potential when charged lipids, such as oleate, are present in sufficient amounts. This additional repulsion could tip the balance and inhibit growth of the mixed micelles. As discussed above, it is not completely clear if the type of neutral fatty lipid will affect the growth of rods.

We attempted to model the mixed micelle growth observed in some of the bile salt−fatty lipid mixtures by using interaction for a "sticky" charged sphere. We used a modified Baxter method for the solution of the Percus−Yevick equation for hard spheres with a short-range attractive potential.[50,55] In this approach, the attractive interaction was described by a potential well at the particle surface of width d and depth $-U_0$. A "stickiness" parameter, τ, is defined such that $\tau = \{4[\exp(U_0/$

$(k_BT)) - 1][(1 + d/R)^3 - 1]\}^{-1}$. The charged, sticky, hard sphere $S(Q)$ was then calculated using the random-phase approximation using an ansantz[56] so that $S(Q) = \{1 + 24\phi[\hat{c}_s(Q,\phi) + \hat{c}_c(Q,\phi)]\}^{-1}$, where $\hat{c}_s$, and $\hat{c}_c$ are, respectively, the Fourier transforms of the sticky, hard sphere potential and a Coulomb potential. We used the RMSA algorithm to calculate $S(Q)$, then substituted the hard sphere contribution to the result, calculated from eq 15, with that calculated for the hard sphere with an attractive potential. At these low volume fractions ($\phi \approx 0.001-0.01$), there was no value of τ where the attractive part of the potential leads to particle growth. As τ_c (the value at which the stickiness parameter becomes sufficiently large to cause the micelles to flocculate) was approached, the system went directly from a single phase of micelles dominated by repulsive interactions to a flocculant. Using this approach, we were able to reproduce the results of earlier studies,[51,55,56] which predicted micelle growth at much higher volume fractions by aggregation of hard, sticky spheres and of charged, sticky spheres. Thus, we were not successful in using the Baxter approach to understand aggregation and growth in the conjugated bile salt−fatty lipid systems at these relatively low concentrations.

Other Phases. In systems containing the trihydroxy bile salt, cholylglycine, there was a concentration-induced transition to SLV's with either monoolein or phosphatidylcholine when the solutions were diluted enough. In both cases the transition included a coexistence region containing elongated or rodlike mixed micelles and SLV's. The mixtures containing the dihydroxy bile salt, chenodeoxycholylglycine, with monoolein differed from counterparts containing EPPC and either chenodeoxycholyltaurine[5] or deoxycholyltaurine[24] by not having a mixed micelle to vesicle transition. Instead, the monoolein-containing system underwent a concentration-dependent transition to what has been identified as cubic[8] and or spongelike phases.[10] In the cholylglycine−monoolein−oleate/oleic acid mixtures there was also a transition to SLV's when the total lipid concentration is lowered sufficiently. An additional transition was observed to an unidentified phase at yet lower concentrations, just as in the solutions containing only monoolein.[8,10,17] We have noted the similarity of the scattering to that observed for putative stacked ribbon or "hole-defect" lamellar phases.[47,48] There may have been a transition to SLV's in the cholylglycine−oleate/oleic acid mixtures below 4.0 g/L, but the evidence is not clear (Figure 12b). One has to question if the models used in this last case were appropriate.

Induction of Curvature by Bile Salts. In previous work we concluded that curvature required for mixed micelle stability was introduced by the bile salt acting as a wedge between the fatty lipid molecules.[17−19] In the model, the bile salt was inserted near the interface between the EYPC or DPPC hydrophilic and hydrophobic regions with the steroid nucleus of the bile salt parallel to the surface. The positive curvature introduced by this interaction was maintained in particles containing monoolein, even though the inherent curvature of the monoolein is negative in this case. Oleate has even more negative curvature than monoolein by virtue of the smaller hydrophobic head, yet even here the bile salt interaction induces sufficient positive curvature to stabilize an oblate cylindrical micelle shape. However, the polydispersity in mixed micelles and the two types of mixed micelle morphology observed here in some of the oleate/oleic acid mixtures showed the interaction between bile salt and oleate/oleic acid to be more ambivalent. This is particularly true in the oleate/oleic acid solution with cholylglycine. This trihydroxy-conjugated bile salt is more hydrophilic than its dihydroxy counterpart, chenodeoxycholylglycine; thus, it is more soluble, and higher concentrations are required to maintain an amount that is needed in the micelle to maintain curvature. This, balanced with what we propose is an energetically favored interaction between the bile salt and the fatty lipid, results in a coexistence between the more favored oblate cylinders and tabletlike forms. The tabletlike forms are likely to consist of bilayer sheets of fatty lipids surrounded by a ribbon of bile salt, like that originally proposed for the bile salt−EYPC mixed micelles[26] and which we have proposed to exist at high pressure.[48,49] As similar coexistence was observed in the chenodeoxycholylglycine mixtures with monoolein and oleate/oleic acid but at much lower concentrations, owing to the significantly lower solubility of this bile salt.

The mechanism of the induction of curvature for rod and vesicle phases proposed above for the bile salt-containing asymmetric systems is different in detail than that proposed for symmetric surfactants.[12] Curvature in symmetric systems, mixtures of anions and cations of flexible, rodlike molecules with alkane hydrophobic tails, results from chain packing densities and the free energy contributions of the headgroups.[12] In the asymmetric systems the curvature is induced by the insertion of the second surfactant. This accounts for the differences in the phase maps the between the two types of systems. At lower ionic strength, the phase maps of symmetric systems are in general symmetric with respect to the concentration of each amphiphile. The vesicle phases occupy two closely spaced lobes extending from the water corner along either side of the solute equimolar line. The relative size and shape of the two lobes on either side of the equimolar line depends on the ionic conditions.[3] Mixed disks and rods or ribbons are present at higher total lipid concentrations, with rods or ribbons being at the extremes in composition. At higher total concentrations, there are liquid crystal lamellar phases along either side of the equimolar line. In the asymmetric systems, the isotropic micellar phase is much larger and the vesicle phase appears only along one side of the equimolar surfactant line, with mixed micelles and mixed phases containing simple micelles on the other side. Hexagonal, lamellar, and other liquid crystal phases predominate when the fatty lipid content is high. The distinct character of the asymmetric systems make the study of their self-assembly essential to the general understanding colloidal complex fluids.

Implications on the Physiology of Bile and Intestinal Content. For the most part, these bile salt colloid systems conserve the particle morphology and structure, even when the fatty components change. This implies that the micelles are very similar in two very different biological liquids—bile and intestinal content. The constituents of the mixed micelles of bile have very different physiological functions. The biliary micelle, which may be termed an "excretory micelle", serves as a vehicle for cholesterol excretion. The intestinal micelle, which may be termed an "absorptive micelle", serves as a vehicle for absorption of dietary lipids (fatty acids, monoglycerides, and fat-soluble vitamins). In both bilary tract and the small intestine, cooperativity in the association of bile salt anions and fatty lipids lowers the intermicellar concentration of bile acid anions, thereby protecting the epithelial membrane from being damaged by the bile acids.[57] These results support the view that, with some minor exceptions, the same particle forms may be found even as conjugated bile acids function as transporters of liver products, as emulsifiers of dietary triglycerides in the intestinal milieu, and as solubilizers of fatty acids and monoglyderides during fat digestion. This conservation of particle form may reflect the role of particle shape in the physiological function of bile components.

Acknowledgment. This work was supported by Laboratory Directed Research and Development Funds conducted under the auspices of the U.S. Department of Energy at the Manuel Lujan Jr. Neutron Scattering Center, Los Alamos Neutron Science Center of the Los Alamos National Laboratory, which is supported by the Office of Basic Energy Sciences of the U.S. Department of Energy under Contract W-7405-Eng-36 to the University of California. Work at UCSD was supported in part by NIH Grant DK 21506 (to A.F.H.). This material is based on activities supported by the National Science Foundation under Agreement No. DMR-9423101. We acknowledge the support of the National Institute of Standards and Technology, U.S. Department of Commerce, in providing the neutron facilities used in this work. This work benefited from the use of the intense pulsed neutron source at Argonne National Laboratory operated under funding from the U.S. Department of Energy, BES-Materials Science, under Contract W-31-109-Eng-38. We thank Dr. C. Glinka (NIST) for expert help in carrying out these measurements.

References and Notes

(1) Hjelm, R. P.; Thiyagarajan, P.; Alkan, M. H. *J. App. Crystallogr*. **1988** , *21*, 858.
(2) Bergstrom, M.; Pedersen, J. S. *Langmuir* **1998**, *14*, 3754.
(3) Bergstrom, M.; Pedersen, J. S. *Langmuir*, **1999**, *15*, 2250.
(4) Brasher, L. L.; Kaler, E. W. *Langmuir* **1996**, *12*, 1670.
(5) Egelhaaf, S. U.; Schurtenberger, P. *J. Phys. Chem.* **1994**, *98*, 8560.
(6) Pedersen, J. S.; Egelhaaf, S. U.; Schurtenberger, P. *J. Phys. Chem.* **1995**, *99*, 1299.
(7) Cohen, D. E.; Thurston, G. M.; Chamberlin, R. A.; Benedek, G. B.; Carey, M. C. *Biochemistry* **1998**, *37*, 14798.
(8) Svärd, M.; Schurtenberger, P.; Fontell, K.; Jönsson, B.; Lindman, B. *J. Phys. Chem*. **1988**, *92*, 2261.
(9) Yaacob, I. I.; Bose, A. *J. Colloid Interface Sci.* **1996**, *178*, 638.
(10) Gustafsson, J.; Nylander, T.; Almgren, M.; Ljusberg-Wahren, H. *J. Colloid Interface Sci.* **1999**, *211*, 326.
(11) Tanford, C. *The Hydrophobic Effect*, 2nd ed.; Wiley: New York, 1980.
(12) Bergstrom, M. *J. Colloid Interface Sci.* **1996**, *181*, 208.
(13) Isrealichvilli, J. N. *Intermolecular and Surface Forces*, 2nd ed.; Academic Press: San Diego, CA 1992.
(14) Hjelm, R. P.; Thiyagarajan, P.; Alkan, M. H. *Mol. Cryst. Liq. Cryst.* **1990**, *A180*, 155.
(15) Hjelm, R. P.; Thiyagarajan, P.; Sivia, D.; Lindner, P.; Alkan, H.; Schwahn, D. *Prog. Colloid Polym. Sci.* **1990**, *81*, 225.
(16) Hjelm, R. P.; Thiyagarajan, P.; Alkan-Onyuksel, H. *J. Phys. Chem.* **1992**, *96*, 8653.
(17) Hjelm, R. P.; Schteingart, C. D.; Hofmann, A. F.; Sivia, D. S. *J. Phys. Chem.* **1995**, *99*, 16395.
(18) Hjelm, R. P.; Thiyagarajan, P.; Schteingart, C. D.; Hofmann, A. F. Alkan-Onyuksel, M. H.; Ton-Nu, H.-T. *Falk Symposium No 80: Bile Acids in Gastroenterology: Basic and Clinical* Advances; Kluwer: Dordrecht, The Netherlands, 1995; pp 41−58.
(19) Hjelm, R. P.; Thiyagarajan, P.; Schteingart, C. D.; Hofmann, A. F.; Alkan-Onyuksel, M. H. In *Neutrons in Biology*; Schoenborn, B. Knott, R., Eds.; Plenum: New York, 1996; pp 175−190.
(20) Hofmann, A. F.; Borgström, B. *J. Clin. Invest.* **1964**, *43*, 247.
(21) Poley, J. R.; Hofmann, A. F. *Gastroenterology* **1976**, *71*, 38.
(22) Cabral, D. J.; Small, D. M. In *Handbook of Physiology, The Gastrointestinal System III*; Schultz, S. G, Forte, J. G., Rauner, B. B., Eds.; Waverly Press: Baltimore, MD, 1989; Section 4, pp 621−662.
(23) Mansbach, C. N.; Cohen, R. S. *J. Clin. Invest.* **1975**, *56*, 1.
(24) Long, M. A.; Kaler, E. W.; Lee, S. P.; Wignall, G. D. *J. Phys. Chem.* **1994**, *98*, 4402.
(25) Long, M. A.; Kaler, E. W.; Lee, S. P. *Biophys. J.* **1994**, *67*, 1733.
(26) Mazer, N. A.; Benedek, G. B.; Carey, M. C. *Biochemistry* **1980**, *19*, 601.
(27) Mazer, N. A.; Schurtenberger, P.; Carey, M. C.; Preisig, R.; Weigand, K.; Kanzig, W. *Biochemistry*. **1984**, *23*, 1994.
(28) Shankland, W. *Chem. Phys. Lipids* **1970**, *4*, 109.
(29) Schurtenberger, P.; Lindeman, B. *Biochemistry* **1985**, *24*, 7161.
(30) Stark, R. E.; Gosselin, G. J.; Donovan, J. M.; Carey, M. C.; Roberts, M. F. *Biochemistry* **1985**, *24*, 5599.
(31) Vinson, P. K.; Talmon, Y.; Walter, A. *Biophys. J.* **1989**, *56*, 669.
(32) Walter, A.; Vinson, P. K.; Talmon, Y. *Biophys. J.* **1991**, *60*, 1315.
(33) Lucassen, J. *J. Phys. Chem.* **1966**, *70*, 1824.
(34) Hjelm, R. P. *J. Appl. Crystallogr.* **1988**, *21*, 618.
(35) Seeger, P. A.; Hjelm, R. P. *J. Appl. Crystallogr.* **1991**, *24*, 467.
(36) Kotlarchyk, M.; Chen, S.-H. *J. Chem. Phys.* **1983**, *79*, 2461.
(37) Hayter, J. P.; Penfold, J. *Mol. Phys.* **1981**, *42***,** 109.
(38) Hansen, J.-P.; Hayter, J. B. *Mol. Phys.* **1982**, *46*, 651.
(39) Ashcroft, W.; Lekner, J. *Phys. Rev.* **1966**, *145*, 83.
(40) Kinning, D. J.; Thomas, E. L. *Macromolecules* **1984**, *17*, 1712.
(41) Hofmann, A. F. *Biochem. J.* **1963**, *89*, 57.
(42) Dreher, K. D.; Schulman, J. H.; Hofmann, A. F. *J. Colloid Interface Sci.* **1967**, *25*, 71.
(43) Skilling, J.; Bryan, R. K. *Mon. Not. R. Astron. Soc.* **1984**, *211*, 111−124.
(44) Gull, S In *Maximum Entropy and Bayesian Methods, Cambridge 1988*; Skilling, J., Ed.; Kluwer: Dordrecht, 1988; pp 53−71.
(45) Skilling, J. In *Maximum Entropy in Action*; Buck, B.; Macaulay, V. A., Eds.; Clarendon Press: Oxford, 1991; pp 19−40.
(46) Charter, M. K.; Gull, S. F. *J. Pharmacokin. Biopharm*. **1991**, *19*, 497.
(47) Mang, J. T.; Hjelm, R. P. *Mol. Cryst. Liq. Cryst.* **1997**, *299*, 439.
(48) Mang, J. T.; Hjelm, R. P. *Int. J. Thermophys.* **1998**, *19*, 461.
(49) Hjelm, R. P. *J. Appl. Crystallagr.* **1985**, *18*, 452.
(50) Baxter, J. *J. Chem. Phys.* **1968**, *49*, 2770.
(51) Hayter, J. P.; Zulauf, M. *Colloid Polym. Sci.* **1982**, *260*, 1023.
(52) Sheu, E. Y.; Wu, C.-F.; Chen, S.-H. *J. Phys. Chem.*, **1986**, *90*, 4179.
(53) Jerke, G.; Pedersen, J. S.; Egelhaaf, S. U.; Schurtenberger, P. *Phys. Rev.* **1997**, *E56*, 5772.
(54) Nichols, J. W.; Ozarowski, J. *Biochemistry* **1990**, *29*, 4600.
(55) Menon, S. V. G.; Manohar, C.; Srinivasa Rao, K. *J. Chem. Phys.* **1991**, *95*, 9186.
(56) Kelkar, V. K.; Mishra, B. K.; Srinivasa Rao, K.; Goyal, P. S.; Manohar, C. *Phys. Rev.* **1991**, *A44*, 8421.
(57) Oude Elferink, R. P. J.; Tyygat, G. N. J.; Groen, A. K. *FASEB J*. **1997**, *11*, 19.